



**HAL**  
open science

## Monitoring restored tropical forest diversity and structure through UAV-borne hyperspectral and lidar fusion

Danilo Roberti Alves De Almeida, Eben North Broadbent, Matheus Pinheiro Ferreira, Paula Meli, Angelica Maria Almeyda Zambrano, Eric Bastos Gorgens, Angelica Faria Resende, Catherine Torres de Almeida, Cibele Hummel Do Amaral, Ana Paula Dalla Corte, et al.

### ► To cite this version:

Danilo Roberti Alves De Almeida, Eben North Broadbent, Matheus Pinheiro Ferreira, Paula Meli, Angelica Maria Almeyda Zambrano, et al.. Monitoring restored tropical forest diversity and structure through UAV-borne hyperspectral and lidar fusion. *Remote Sensing of Environment*, 2021, 264, pp.112582. 10.1016/j.rse.2021.112582 . hal-03334289

**HAL Id: hal-03334289**

**<https://hal.inrae.fr/hal-03334289v1>**

Submitted on 4 Sep 2024

**HAL** is a multi-disciplinary open access archive for the deposit and dissemination of scientific research documents, whether they are published or not. The documents may come from teaching and research institutions in France or abroad, or from public or private research centers.

L'archive ouverte pluridisciplinaire **HAL**, est destinée au dépôt et à la diffusion de documents scientifiques de niveau recherche, publiés ou non, émanant des établissements d'enseignement et de recherche français ou étrangers, des laboratoires publics ou privés.

## Monitoring restored tropical forest diversity and structure through UAV-borne hyperspectral and lidar fusion

Almeida, Danilo Roberti Alves de; Broadbent, Eben North; Ferreira, Matheus Pinheiro; Meli, Paula; Zambrano, Angelica Maria Almeida; Gorgens, Eric Bastos; Resende, Angelica Faria; Almeida, Catherine Torres de; Amaral, Cibele Hummel do; Corte, Ana Paula Dalla; Silva, Carlos Alberto; Romanelli, João P.; Prata, Gabriel Atticciati; Papa, Daniel de Almeida; Stark, Scott C.; Valbuena, Ruben; Nelson, Bruce Walker; Guillemot, Joannes; Féret, Jean-Baptiste; Chazdon, Robin; Brancalion, Pedro H.S.

### Remote Sensing of Environment

DOI:  
[10.1016/j.rse.2021.112582](https://doi.org/10.1016/j.rse.2021.112582)

Published: 01/10/2021

Peer reviewed version

[Cyswllt i'r cyhoeddiad / Link to publication](#)

*Dyfyniad o'r fersiwn a gyhoeddwyd / Citation for published version (APA):*  
Almeida, D. R. A. D., Broadbent, E. N., Ferreira, M. P., Meli, P., Zambrano, A. M. A., Gorgens, E. B., Resende, A. F., Almeida, C. T. D., Amaral, C. H. D., Corte, A. P. D., Silva, C. A., Romanelli, J. P., Prata, G. A., Papa, D. D. A., Stark, S. C., Valbuena, R., Nelson, B. W., Guillemot, J., Féret, J.-B., ... Brancalion, P. H. S. (2021). Monitoring restored tropical forest diversity and structure through UAV-borne hyperspectral and lidar fusion. *Remote Sensing of Environment*, 264, Article 112582. <https://doi.org/10.1016/j.rse.2021.112582>

#### Hawliau Cyffredinol / General rights

Copyright and moral rights for the publications made accessible in the public portal are retained by the authors and/or other copyright owners and it is a condition of accessing publications that users recognise and abide by the legal requirements associated with these rights.

- Users may download and print one copy of any publication from the public portal for the purpose of private study or research.
- You may not further distribute the material or use it for any profit-making activity or commercial gain
- You may freely distribute the URL identifying the publication in the public portal ?

#### Take down policy

If you believe that this document breaches copyright please contact us providing details, and we will remove access to the work immediately and investigate your claim.

1 **Monitoring restored tropical forest diversity and structure through UAV-borne**  
2 **hyperspectral and lidar fusion**

3  
4 Danilo Roberti Alves de Almeida<sup>1,2</sup>; Eben North Broadbent<sup>2</sup>; Matheus Pinheiro Ferreira<sup>3</sup>; Paula Meli<sup>4</sup>;  
5 Angelica Maria Almeyda Zambrano<sup>5</sup>; Eric Bastos Gorgens<sup>6</sup>; Angelica Faria Resende<sup>1</sup>; Catherine Torres  
6 de Almeida<sup>1</sup>; Cibele Hummel do Amaral<sup>7</sup>; Ana Paula Dalla Corte<sup>8</sup>; Carlos Alberto Silva<sup>9, 10</sup>; João P.  
7 Romanelli<sup>1</sup>; Gabriel Atticciati Prata<sup>2</sup>; Daniel de Almeida Papa<sup>11</sup>; Scott C. Stark<sup>12</sup>; Ruben Valbuena<sup>13</sup>;  
8 Bruce Walker Nelson<sup>14</sup>; Joannes Guillemot<sup>1, 15, 16</sup>; Jean-Baptiste Féret<sup>17</sup>; Robin Chazdon<sup>18</sup>; Pedro H. S.  
9 Brancalion<sup>1</sup>

10  
11  
12 <sup>1</sup> Department of Forest Sciences, “Luiz de Queiroz” College of Agriculture, University of São Paulo  
13 (USP/ESALQ), Piracicaba, SP, Brazil

14 <sup>2</sup> Spatial Ecology and Conservation Lab, School of Forest Resources and Conservation, University of  
15 Florida, Gainesville, FL, USA

16 <sup>3</sup> Cartographic Engineering Department, Military Institute of Engineering (IME), Rio de Janeiro, RJ,  
17 Brazil

18 <sup>4</sup> Landscape Ecology and Conservation Lab (LEPCON), Universidad de La Frontera, Temuco, Chile

19 <sup>5</sup> Spatial Ecology and Conservation (SPEC) Lab, Center for Latin American Studies, University of  
20 Florida, Gainesville, FL, USA

21 <sup>6</sup> Department of Forestry, Federal University of Jequitinhonha e Mucuri Valleys (UFVJM), Diamantina,  
22 Minas Gerais, Brazil

23 <sup>7</sup> Department of Forest Engineering, Federal University of Viçosa, Viçosa, Minas Gerais, Brazil

24 <sup>8</sup> Department of Forest Engineering, Federal University of Paraná, Curitiba, Brazil

25 <sup>9</sup> School of Forest, Fisheries and Geomatics Sciences, University of Florida, Gainesville, FL, USA

26 <sup>10</sup> Department of Geographical Sciences, University of Maryland, College Park, USA;

27 <sup>11</sup> Embrapa Acre, Rio Branco, Acre, Brazil

28 <sup>12</sup> Department of Forestry, Michigan State University, East Lansing, MI, USA

29 <sup>13</sup> School of Natural Sciences, Bangor University, Bangor, UK

30 <sup>14</sup> National Institute for Amazon Research (INPA), Manaus, AM, Brazil

31 <sup>15</sup> CIRAD, UMR Eco&Sols, F-34398 Montpellier, France

32 <sup>16</sup> Eco&Sols, Univ Montpellier, CIRAD, INRAE, Institut Agro, IRD, Montpellier, France

33 <sup>17</sup> TETIS, INRAE, AgroParisTech, CIRAD, CNRS, Université Montpellier, Montpellier, France

34 <sup>18</sup> Tropical Forests and People Research Centre, University of the Sunshine Coast, Sippy Downs-QLD  
35 4556, Australia

54 **ABSTRACT**

55

56 Remote sensors, onboard orbital platforms, aircraft, or unmanned aerial vehicles (UAVs) have  
57 emerged as a promising technology to enhance our understanding of changes in ecosystem  
58 composition, structure, and function of forests, offering multi-scale monitoring of forest  
59 restoration. UAV systems can generate high-resolution images that provide accurate  
60 information on forest ecosystems to aid decision-making in restoration projects. However,  
61 UAV technological advances have outpaced practical application; thus, we explored combining  
62 UAV-borne lidar and hyperspectral data to evaluate the diversity and structure of restoration  
63 plantings. We developed novel analytical approaches to assess twelve 13-year-old restoration  
64 plots experimentally established with 20, 60 or 120 native tree species in the Brazilian Atlantic  
65 Forest. We assessed (1) the congruence and complementarity of lidar and hyperspectral-  
66 derived variables, (2) their ability to distinguish tree richness levels and (3) their ability to  
67 predict aboveground biomass (AGB). We analyzed three structural attributes derived from lidar  
68 data—canopy height, leaf area index (LAI), and understory LAI—and eighteen variables  
69 derived from hyperspectral data—15 vegetation indices (VIs), two components of the  
70 minimum noise fraction (related to spectral composition) and the spectral angle (related to  
71 spectral variability). We found that VIs were positively correlated with LAI for low LAI values,  
72 but stabilized for LAI greater than 2 m<sup>2</sup>/m<sup>2</sup>. LAI and structural VIs increased with increasing  
73 species richness, and hyperspectral variability was significantly related to species richness.  
74 While lidar-derived canopy height better predicted AGB than hyperspectral-derived VIs, it was  
75 the fusion of UAV-borne hyperspectral and lidar data that allowed effective co-monitoring of  
76 both forest structural attributes and tree diversity in restoration plantings. Furthermore,  
77 considering lidar and hyperspectral data together more broadly supported the expectations of  
78 biodiversity theory, showing that diversity enhanced biomass capture and canopy functional  
79 attributes in restoration. The use of UAV-borne remote sensors can play an essential role during

80 the UN Decade of Ecosystem Restoration, which requires detailed forest monitoring on an  
81 unprecedented scale.

82

83 **Keywords:** forest landscape restoration, tropical forests, drones, lidar remote sensing,  
84 hyperspectral remote sensing, leaf area density, vegetation indices

## 1. INTRODUCTION

An ambitious restoration agenda has been set to increase forest cover in deforested and degraded landscapes, to improve their multifunctionality and capacity to provide essential ecosystem services, such as maintaining biodiversity, water supply and carbon storage (Erbaugh & Oldekop 2018). Forest monitoring will play a crucial role to track the success of these goals and also support adaptive management (Brancalion & Holl 2020; Fagan et al. 2020), given the widespread failures in ecosystem restoration and the unprecedented scale of restoration pledges (Versluijs et al. 2019; Chagas et al. 2020). Currently, there is a pressing need to develop social collaborative and effective technologies for monitoring ecosystem recovery over large areas (hundreds to millions of hectares) using multiple key ecological indicators (Guariguata & Evans 2020; Höhl et al. 2020). Remote sensors onboard orbital platforms, aircraft, or unmanned aerial vehicles (UAVs) have emerged as promising technologies to upscale forest restoration monitoring. Particularly, UAV systems can generate high-resolution images that provide accurate information on forest stands with or without the need for ground-based data (e.g., calibration or validation) to estimate important forest attributes such as the number of trees, aboveground biomass, or canopy openness (Almeida et al. 2020a, Kotivuori et al. 2020; Ferreira et al. 2020).

Accurate methods to estimate forest attributes to support decision-making are required for the effective remote monitoring of forests undergoing restoration (Almeida et al. 2019a). For example, forest cover, biomass stock and tree species diversity vary along forest successional sequences and are commonly employed to monitor forest restoration (Wortley et al. 2013). To this aim, multispectral sensors have proven useful, offering estimates of these critical variables. However, a high leaf area index (LAI) saturates most vegetation indices (VIs) derived from remote sensing (Turner et al. 1999). This saturation complicates their use to monitor structural attributes (such as aboveground biomass - AGB) in high-LAI tropical

111 forests, which account for a large portion of global restoration commitments (Timothy et al.  
112 2016, Crouzeilles et al. 2019). On the other hand, the light detection and ranging (lidar) sensor  
113 has been hailed as a promising technology for retrieving forest canopy structural attributes,  
114 regardless of canopy leaf area density. Lidar enables the estimation of canopy structural  
115 attributes with high precision and accuracy, such as vegetation density in the understory, LAI,  
116 tree height, the identification and measurement of forest gaps, and AGB (Almeida et al. 2019b,  
117 da Costa et al. 2020, Valbuena et al. 2020, Dalagnol et al. 2021). On the other hand, lidar  
118 technology is of limited use for assessing tree species diversity, for which hyperspectral has  
119 shown greater potential (Asner & Martin 2009).

120         Assessing the different facets of forest diversity, such as tree richness, functional  
121 diversity, and composition, is one of the most important but challenging modern remote sensing  
122 tasks (Asner et al. 2015). With lidar, one approach is to use canopy structural attributes as  
123 predictive variables for indirectly estimating tree species diversity (Hernández-Stefanoni et al.  
124 2014, Ali et al. 2019, De Cáceres et al. 2019, Adhikari et al. 2020). Notably, a more species-  
125 rich forest is expected to have a more heterogeneous and complex canopy structure (Zellweger  
126 et al. 2019, Mensah et al. 2020). Secondary forests with higher biomass are expected to have  
127 reached a later stage of succession, supporting more tree species (Gamfeldt et al. 2013, Lasky  
128 et al. 2014, Finegan et al. 2015, Poorter et al. 2015). However, structure–richness relationships  
129 are not ubiquitous and depend on a wide range of factors, such as forest type, management, use  
130 and disturbance history. Consequently, the lidar approach has so far demonstrated a limited  
131 ability for local scale prediction of species richness, especially in hyper-diverse tropical biomes  
132 (Marselis et al. 2020, Almeida et al. 2019a, Valbuena et al. 2020).

133         Hyperspectral imaging (HSI) has a significant potential for estimating or measuring  
134 taxonomical and functional diversity of highly diverse tropical forests (Feret & Asner 2014;  
135 Vaglio Laurin et al. 2016; Durán et al. 2019). HSI measures reflected radiation from the forest

136 canopy over hundreds of narrow spectral bands (or channels) within the visible- to short-wave  
137 infrared wavelength range (VSWIR, 400-2500 nm). The rationale for using hyperspectral  
138 sensors to discriminate species-richness is that each species (or group of species) has specific  
139 combinations of spectral features. These include absorption by specific chemical constituents  
140 of leaves and non-photosynthetic elements and scattering driven by vegetation structure at  
141 different scales, such as leaf anatomy, leaf area index, leaf angle distribution function (Ferreira  
142 et al. 2016). However, this combination of spectral traits does not necessarily result in a unique  
143 species-specific spectral identity (and thus perfect discrimination among species), as significant  
144 intraspecific variability in spectral traits was evidenced (Amaral et al. 2018; Camarretta et al.  
145 2020). For example, a single species' spectral characteristics can vary widely depending on  
146 environmental variables (e.g., water availability) or species and community attributes (e.g., leaf  
147 amount and leaf age) (Yan et al. 2018; Ferreira et al. 2019; Gonçalves et al. 2020). Another  
148 rationale is that the spectral heterogeneity is related to tree species diversity and composition  
149 (Rocchini et al. 2010; Féret and Asner, 2014; Asner et al. 2017; Laliberté et al. 2020). HSI also  
150 enables linking canopy reflectance to biophysical and chemical properties using various  
151 approaches, including narrow-band vegetation indices, which are designed to be used as  
152 proxies for both structural (e.g., vegetation density) and physiological (e.g., leaf chemical  
153 composition and water stress) properties (Zhao et al. 2018).

154         Using HSI data to study species diversity or the retrieval of canopy chemical properties  
155 is still challenging, particularly in tropical ecosystems due to their high biodiversity and  
156 structural complexity (Féret and Asner 2013). HSI data acquisition with airborne surveys is  
157 usually costly, planning intensive, and may be operationally prohibitive in places with poor  
158 infrastructure and resources, such as in some tropical forest regions. Conversely, restoration  
159 practitioners face the challenges of monitoring tree diversity in tropical forest regions  
160 (Crouzeilles et al. 2019), given the difficulty of properly identifying hundreds of tree species

161 and the reduced accessibility of restoration areas for forest inventories (Keil et al. 2019). As  
162 restoration programs are usually composed of several small to mid-size polygons scattered  
163 across large and heterogeneous areas, airborne surveys are less viable.

164         Recent technological developments have allowed for manufacturing UAV-compatible  
165 HSI sensors, a promising approach to mainstreaming the common use of HSI in tropical forest  
166 restoration monitoring. UAVs are a technological frontier of remote sensing data acquisition  
167 and may constitute an alternative to high-cost airborne hyperspectral and lidar campaigns. The  
168 use of UAV-borne remote sensors, both lidar and HSI, nonetheless presents pros and cons. The  
169 main advantage is the higher spatial resolution. Point cloud density from airborne lidar usually  
170 ranges between 0.4 and 30 points per m<sup>2</sup> (ppm<sup>2</sup>), whereas UAV lidar acquisitions can reach  
171 100-1000 ppm<sup>2</sup> (d'Oliveira et al. 2020; Prata et al. 2020). The high point density increases the  
172 accuracy of estimating structural parameters, such as vertical profiles of leaf area density  
173 (Almeida et al. 2019c). It can even allow the individualization of trees and measurement of  
174 stem volume in open-canopy forests such as eucalyptus plantations (Corte et al. 2020) and  
175 temperate forests (Kruček et al. 2020). For UAV-HSI, the centimetric resolution of the pixels  
176 allows a better characterization of target objects, detecting vegetation-free patches, removing  
177 background contribution, and capturing the spectral variability within and among crowns.  
178 Conversely, flight instability of the UAV, changing view and illumination geometry and  
179 changing sky conditions make the use of these images challenging. HSI reflectance retrievals  
180 from UAVs require a matched incident radiance HSI sensor and non-trivial pre-processing  
181 steps, including corrections for bidirectional reflectance distribution function (BRDF) and  
182 atmospheric effects (Jia et al. 2020).

183         To date, few investigations have assessed the potential of UAV-lidar-HSI systems in  
184 tropical forest monitoring. Sankey et al. (2017) and Lin et al. (2019) used UAV-lidar-HSI  
185 systems to monitor semi-arid and pine forests, respectively. Here, we explored the fusion of

186 UAV-borne lidar and hyperspectral data to remotely access the structure and diversity of  
187 restored tropical forests. We developed a novel analytical approach for a mixed-species, 13-  
188 year-old restoration plantation experimentally established with 20, 60, and 120 native tree  
189 species in the Brazilian Atlantic Forest. Specifically, we assessed (1) the congruence of lidar  
190 and hyperspectral variables, (2) their usefulness to distinguish tree species richness levels, and  
191 (3) their ability to predict aboveground biomass. Our work goes well beyond traditional  
192 measurements based on sampling plots, providing high-accuracy and precision information for  
193 upscaling field variables to satellite-based hyperspectral and lidar observations, representing  
194 an effective strategy for large-scale forest restoration monitoring during the United Nations  
195 Decade on Ecosystem Restoration (2021-2030).

196  
197  
198  
199  
200  
201  
202

## **2. METHODS**

### **2.1. Experimental site and field data**

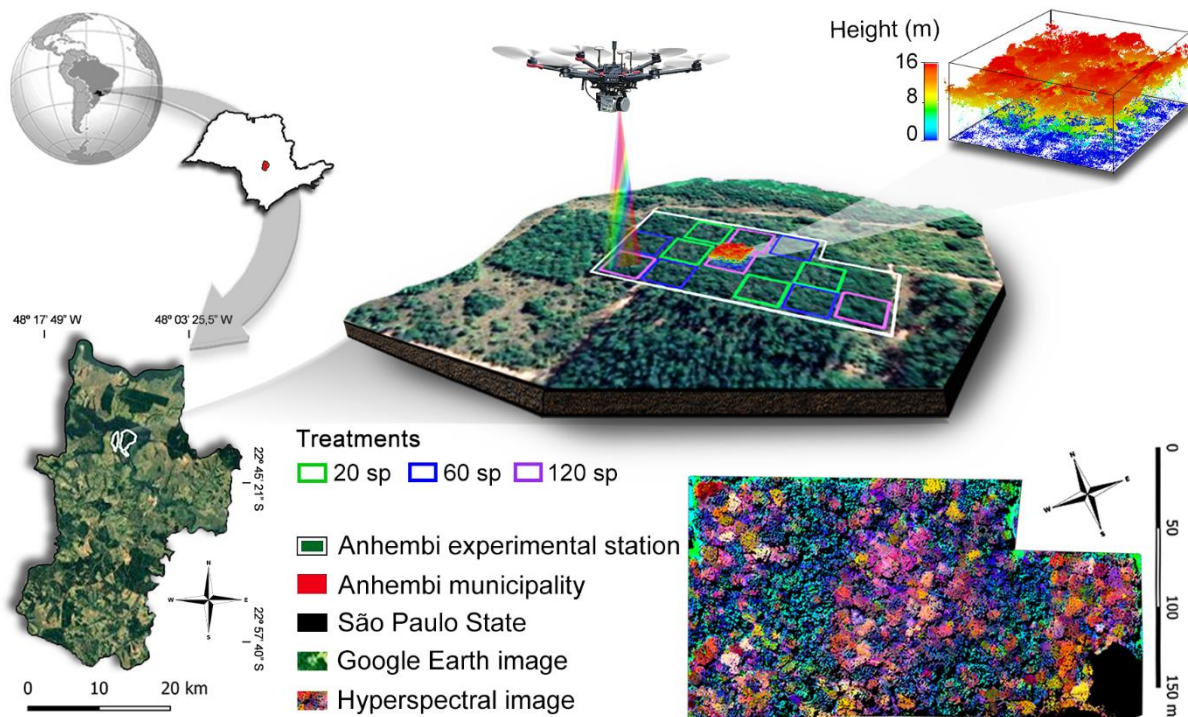
202 We used an experimental mixed-species restoration plantation with three diversity  
203 levels to explore the potential and limitations of fusing UAV-borne lidar and hyperspectral data  
204 to assess structure and diversity. The experimental plots were established in May 2006 in  
205 Anhembi-SP, southeastern Brazil, in a completely randomized design with 20, 60, and 120  
206 native tree species (hereafter sp.), each with four replicates, in 45 x 48 m plots. The area was  
207 previously covered by pastures, with no regeneration of native tree species. Tree seedlings were  
208 randomly planted with 3 x 1.5 m spacing and ensuring a homogeneous density across species.  
209 The species pool present in the treatments with the lowest richness was contained in the  
210 treatments with higher richness, i.e., species of the treatment of 20 species are contained in the  
211 treatment of 60 species, which are also contained in the treatment of 120 species. Extensive  
212 information on the study site and experiment is provided by Duarte et al. (2021). Due to the  
213 low coverage of HSI in one plot, the treatment of 120 species had only three replicates for the

214 analysis using HSI data. Forest inventory field data were collected in November 2019, when  
 215 the plantation was 13.5 years old. At this time, 58 and 114 species had survived in the 60- and  
 216 120 species treatments, respectively. For all living stems, we identified the tree species in this  
 217 inventory, measured diameter 30 cm above the ground and measured total height. We used the  
 218 allometric equation developed by Ferez et al. (2015) for a neighboring restoration plantation to  
 219 estimate aboveground woody biomass of each individual (equation 1). Wood densities were  
 220 obtained for all tree species based on wood discs (cross-sections from the stem) sampled in  
 221 destructive plots established, using three individuals per species (see Ferez, 2012 for more  
 222 details).

223  
 224 
$$\ln(\text{AGB}_W) = 6.039 + 0.945 \times \ln(\text{SA}) + 0.961 \times \ln(\text{Ht}) + 1.022 \times \ln(\rho) \quad (1)$$
  
 225

226 Where: AGB<sub>w</sub> = Aboveground woody biomass (Mg/ha); SA: sectional area of the stem (m<sup>2</sup>);  
 227 Ht: total height (m);  $\rho$  = wood density (g/cm<sup>3</sup>).

228



229  
 230 **Figure 1** - Study area and plot designs. Left) site location; upper right) sample design and lidar  
 231 point cloud example of one plot; bottom right) hyperspectral image colored by a false RGB  
 232 composition using the first components from the minimum noise fraction transformation.

233  
234  
235  
236  
237  
238  
239  
240  
241  
242  
243  
244  
245  
246  
247  
248  
249  
250  
251  
252  
253  
254  
255  
256  
257  
258

## 2.2. UAV-borne lidar and hyperspectral data

Data were collected using the GatorEye Unmanned Flying Laboratory, consisting of a hardware system with custom algorithm workflows incorporating lidar, hyperspectral, thermal, and visual (RGB) sensors. The hardware and processing workflows are described in detail in the GatorEye overview manuscript (Broadbent et al. 2021) available at [www.gatoreye.org](http://www.gatoreye.org). The data is also available under the section “2019 Brazil Sao Paulo State August/082819”.

The system uses a DJI Matrice 600 Pro hexacopter platform, with mission planning conducted using Universal Ground Control Station (UGCS) software. GNSS base station data are collected within 3 km of data collection areas, then post-processed online via the Trimble CenterPoint RTX platform, providing typically < 2cm 3D uncertainty within a 2-hour collection period (and < 0.25 cm within 4+ hour collections). The computational sensor core is based on a Phoenix Ultra Scout, a Novatel STIM 300 IMU tactical grade and differential GNSS system. Integrated into this is a (a) Velodyne VLP-32c Ultra Puck LiDAR sensor, (b) Nano VNIR Hyperspectral Headwall sensor (640 pixels x 270 spectral bands in a 100-hertz line scan approach), (c) high-resolution RGB camera, (d) radiometric thermal camera, and (e) time-synchronized downwelling hyperspectral Ocean Optics Flame (upward viewing spectrometer, 400-1025nm wavelength range, and 1.70 nm spectral resolution) (Figure S1). See Broadbent et al. (2021) for more details.

The Velodyne Ultra Puck sensor features 32 individual 905 nm lasers, situated to provide a 360° horizontal (cross-track) and 40° vertical (along-track) field of view. The Ultra Puck fires 600,000 times per second, recording for each pulse the strongest and the last (dual) return, for a theoretical points/sec of 1,200,000 at a range of up to 200 meters. The Headwall Photonics Nano VNIR 270 spectral band lab-calibrated radiance hyperspectral sensor acquires 1400 spectral bands from 400-1000 nm every 0.5 seconds and allows conversion of radiance

259 to reflectance by ratioing with the spectral bands most similar in wavelength from the upward-  
260 facing Ocean Optics Flame sensor (Broadbent et al. 2021).

261 The GatorEye overflew the experimental area 27-30 Aug of 2019 at approximately  
262 solar noon at an aboveground mean altitude of 100 meters. The local solar zenith angle was 32  
263 degrees at solar noon (based on the date 28 Aug 2019, lat, long = -22.75, -48.11). Four flight  
264 lines were acquired to cover the majority of plots. The speed was 12-14 m/s, resulting in a  
265 forward pitch of approximately 12 degrees during flight. Acquisitions were performed under  
266 clear sky conditions with no atmospheric haze. The specific lidar and hyperspectral GatorEye  
267 deliverables used in this study were: (a) the Canopy Height Model (CHM), (b) the cleaned lidar  
268 point cloud, and (c) the ‘reflectance-calibrated hyperspectral shade-filtered orthomosaic’ (e.g.,  
269 HSI image).

270 Lidar flight lines were processed to standard products using the GatorEye Multi-scalar  
271 Post-Processing workflow -- using the software Lastools (Isenburg, 2020) and “lidR” R  
272 package (Roussel & Auty, 2019). This procedure automatically merges flight lines, classifies  
273 ground points and removes noise -- to generate the cleaned point clouds and the rasters DTM  
274 (digital terrain model), DSM (digital surface model) and CHM. More details are given in  
275 Almeida et al. (2019b and 2020). The point density of the final lidar point cloud was  $360 \pm 137$   
276 (mean  $\pm$  *SD*) ppm<sup>2</sup>, of which 80.4% were first returns.

277 Hyperspectral data were processed in three steps. (1) The non-orthorectified time-  
278 synchronized lab-calibrated radiance data from the downward-facing boresighted Nano  
279 hyperspectral camera was projected onto the DSM from the lens using a ray-tracing algorithm.  
280 (2) The radiance bands were then converted to reflectance using the also time-synchronized  
281 and lab-calibrated upward-facing Flame hyperspectral irradiance sensor. (3) The shade was  
282 removed through a separate process where solar geometry was calculated and then applied,  
283 through a ray tracing algorithm (Broadbent et al. 2021), to map portions of the DSM to be

284 either in full sunlight or in the shade at the moment of data acquisition. Shaded pixels were  
285 masked in the final hyperspectral reflectance orthomosaic. Hyperspectral images are  
286 orthorectified onto the lidar derived digital surface models using a custom ray tracing workflow  
287 (Broadbent et al. 2021). The spatial resolution of the final HSI image was 0.20 m. We  
288 performed additional filtering on the hyperspectral data using a 0.20 m moving window filter  
289 across the CHM to remove pixels with a height below four meters. This filtering enabled us to  
290 restrict the spectral data to vegetation targets when estimating tree species compositional values  
291 versus being dominated by the ground level exposed soil spectra which greatly differ from  
292 vegetation.

293         The bidirectional reflectance distribution function (BRDF) describes the variations in  
294 reflectance or radiance intensity measured by a sensor as a function of (1) the angle of  
295 separation of two vectors - view and illumination - and of (2) forward-scatter (viewing toward  
296 the sun) and backscatter (sun behind the viewer). In remotely sensed imagery, BRDF  
297 significantly impacts the retrieval of biophysical surface properties (Wanner et al. 1995). We  
298 corrected the HSI orthomosaic for BRDF effects using a kernel-driven approach. More details  
299 can be found in the Supplementary Material.

300  
301

### 302         **2.3. Data processing and analysis**

303  
304

305         Post-deliverables data processing was performed in the R environment (R Core Team  
306 2020). Three structural attributes were derived from lidar data: canopy height, leaf area index  
307 - LAI, and leaf area index in the understory - LAI.under. (Table 1). At the plot level, we  
308 calculated the mean canopy height and its heterogeneity (standard deviation). The canopy  
309 height was obtained directly from the CHM (0.20 m resolution). To calculate canopy height,  
310 the cloud pulse density was not filtered to a standard density, ensuring the highest accuracy.  
Nonetheless, Silva et al. (2017) have shown that the accuracy of canopy height estimate in

311 Amazon forests stabilizes when pulse density reaches 4 ppm<sup>2</sup>. The LAI (1m resolution) was  
312 calculated from the leaf area density (LAD) estimated using the *lad.voxels* function from the  
313 “leafR” package (Almeida et al. 2019d). The LAI is the sum of the entire LAD vertical profile,  
314 and the LAI understory is the sum of the LAD vertical profile between 1-5 meters in height.  
315 To improve the accuracy of the LAD estimates and remove lidar pulse density bias, the  
316 normalized lidar cloud was filtered to first returns only and then homogenized to 30 ppm<sup>2</sup>  
317 before the LAD calculation. Almeida et al. (2019c) found that higher pulse densities result in  
318 higher LAI estimates in tropical forests. While this bias is small when pulse densities exceed  
319 20 ppm<sup>2</sup>, for all LAI and LAD estimates we elected to standardize to 30 ppm<sup>2</sup> using a  
320 homogenizing filter. The method used to estimate the LAD uses the MacArthur-Horn equation  
321 (MacArthur and Horn 1969) and is based on the Beer-Lambert law, i.e., the attenuation of the  
322 energy transmission rate (lidar pulses) between the canopy vertical strata. See Almeida et al.  
323 (2019c) for more details.

324 A total of 18 variables derived from HSI data were calculated (Table 1): 15 vegetation  
325 indices (VIs), the first two components of the minimum noise fraction (MNF) transformation  
326 (related to spectral composition), and the spectral angle (related to spectral variability). VIs  
327 were divided into four categories: (i) Structural, (ii) Chlorophyll, (iii) Anthocyanin /  
328 Carotenoid, and (iv) Physiology. MNF is a linear transformation of the original HSI data that  
329 applies two cascaded PCA and maximizes the signal/noise ratio (Green et al. 1988). We  
330 performed MNF using ENVI software version 5.3.

331 To assess if species diversity is related to canopy spectral diversity, we computed the  
332 spectral angle between all pairwise combinations of the pixels of each treatment. The spectral  
333 angle ( $\theta$ ) is a suitable measure of the spectral variability (Richer et al. 2016; Ferreira et al.  
334 2018), and was computed as follows, according to Price (1994):

335  
336

$$\theta = \cos^{-1} \left( \frac{\int_{\lambda_a}^{\lambda_b} X(\lambda)Y(\lambda)d\lambda}{\left[ \int_{\lambda_a}^{\lambda_b} X(\lambda)^2 d\lambda \right]^{1/2} \left[ \int_{\lambda_a}^{\lambda_b} Y(\lambda)^2 d\lambda \right]^{1/2}} \right) \quad (2)$$

337  
 338 where  $\theta$  is the spectral angle, measured in radians, between the spectral reflectance of the pixel  
 339  $X$  and the pixel  $Y$  in the spectral interval  $\lambda_a$  to  $\lambda_b$ , i.e., 400 to 1000 nm. The spectral angle was  
 340 computed with sunlit foliated canopy pixels that were selected using NDVI >0.8 and canopy  
 341 height >4m. We used sunlit foliated canopy pixels to avoid the influence of non-photosynthetic  
 342 canopy elements (e.g., branches) in the quantification of spectral diversity. Non-photosynthetic  
 343 vegetation causes variations in the spectral amplitude, that is, brightness differences that may  
 344 increase the spectral variability even if the spectral shapes were the same.

345  
 346 **Table 1.** Variables and their respective descriptions and references. “p” indicates reflectance  
 347 of a hyperspectral band, followed by its wavelength center in nanometers.

	Variable	Description	Reference
<b>Field-derived</b>	Aboveground biomass - AGB (Kg)	Equation 1	Ferez et al. 2015
	<i>Canopy structural attribute</i>		
<b>Lidar-derived</b>	Canopy height - CH (m)	Mean of canopy height model	Almeida et al. 2019b
	Leaf area index - LAI	Sum of leaf area density profile	Almeida et al. 2019c
	LAI understory - LAI.under	Sum of leaf area density profile (1-5 m)	Almeida et al. 2019b
<i>Structural VIs</i>			
	Vegetation Atmospherically Resistant Index (VARI)	$(\rho_{557} - \rho_{643}) / (\rho_{557} + \rho_{643} - \rho_{465})$	Gitelson et al. 2002a
	Simple Ratio (SR)	$\rho_{865} / \rho_{672}$	Jordan et al. 1969
	Normalized Difference Vegetation Index (NDVI)	$(\rho_{865} - \rho_{672}) / (\rho_{865} + \rho_{672})$	Rouse et al. 1974
	Enhanced Vegetation Index (EVI)	$2.5 \times ((\rho_{865} - \rho_{672}) / (\rho_{865} + 6 \times \rho_{672} - 7.5 \times \rho_{464} + 1))$	Huete et al. 2002
<i>Chlorophyll VIs</i>			
	Structurally Insensitive Pigment Index (SIPI)	$(\rho_{800} - \rho_{445}) / (\rho_{800} + \rho_{680})$	Peñuelas 1995
	Chlorophyll Absorption in Reflectance Index (CARI)	$(\rho_{700} - \rho_{670}) - 0.2 \times (\rho_{700} - \rho_{550})$	Kim (1994)
	Chlorophyll Red-Edge Index (CI.rededge)	$\rho_{851} / \rho_{730} - 1$	Gitelson et al. 2006
	Chlorophyll Green Index (CI.green)	$\rho_{730} / \rho_{531} - 1$	Gitelson et al. 2006
<i>Anthocyanin VIs</i>			
<b>HSI-derived</b>	Modified Anthocyanin Reflectance Index (mARI)	$(1 / \rho_{551}) - (1 / \rho_{701})$	Gitelson et al. 2006
	Anthocyanin Content Index (ACI)	$\rho_{531} / \rho_{941}$	van den Berg and Perkins 2005
<i>Carotenoid VI</i>			
	Carotenoid Reflectance Index (CRI)	$(1 / \rho_{511}) - (1 / \rho_{551})$	Gitelson et al. 2007
<i>Physiology VIs</i>			
	Photochemical Reflectance Index (PRI)	$(\rho_{531} - \rho_{571}) / (\rho_{531} + \rho_{571})$	Gamon et al. 1997
	Red-edge Vegetation Stress Index (RVSI)	$(\rho_{712} + \rho_{753}) / 2 - \rho_{733}$	Merton et al. 1999
	Red edge position (REP)	Max first derivative: 680–750 nm	Horler et al. 1983
	Water Band index (WBI)	$\rho_{900} / \rho_{X970}$	Peñuelas et al. 1997
<i>Spectral composition</i>			
	MNF.1	First component of minimal noise fraction	Green et al. 1988
	MNF.2	Second component of minimal noise fraction	Green et al. 1988
<i>Spectral heterogeneity</i>			
	Spectral angle	Equation 2	Price 1994

348  
349

350 We used Spearman's correlation diagram to assess the relationship between the VIs  
351 (HSI-derived) and the canopy structural variables (lidar-derived). This analysis was performed  
352 at the pixel level (0.20 m resolution). The variables AGB (field-derived) and spectral angle  
353 (HSI-derived) were evaluated at the plot level. For comparing the spectral angle, only the  
354 highest spectral angles of each plot (percentile 90%) were considered. This ensures that the test  
355 assesses the most significant differences within the plots. To determine the relationship of the  
356 variables with the tree species richness levels (treatments), we performed ANOVA and post-  
357 hoc Tukey tests (plot-level analysis). For these analyses, we considered the variables' mean  
358 value and standard deviation within the plots, and the latter was used to describe the

359 heterogeneity of each variable within plots. Finally, the predictive power of AGB from lidar  
360 and HSI variables was evaluated using simple and multiple ordinary least square regressions.  
361 To identify and eliminate outliers, we used t tests based on studentized residuals implemented  
362 using the function outlier.test in R package “car” (Fox & Weisberg, 2019). The assessment of  
363 model accuracy was performed by a leave-one-out cross-validation (LOOCV) procedure  
364 (Almeida et al. 2020a). The relationship between the observed and predicted (via LOOCV)  
365 values were evaluated by testing their 1:1 correspondence under the null hypothesis that their  
366 regression intercept and slope were 0 and 1, respectively (Valbuena et al. 2017).

367

368

### 369 **3. RESULTS**

370

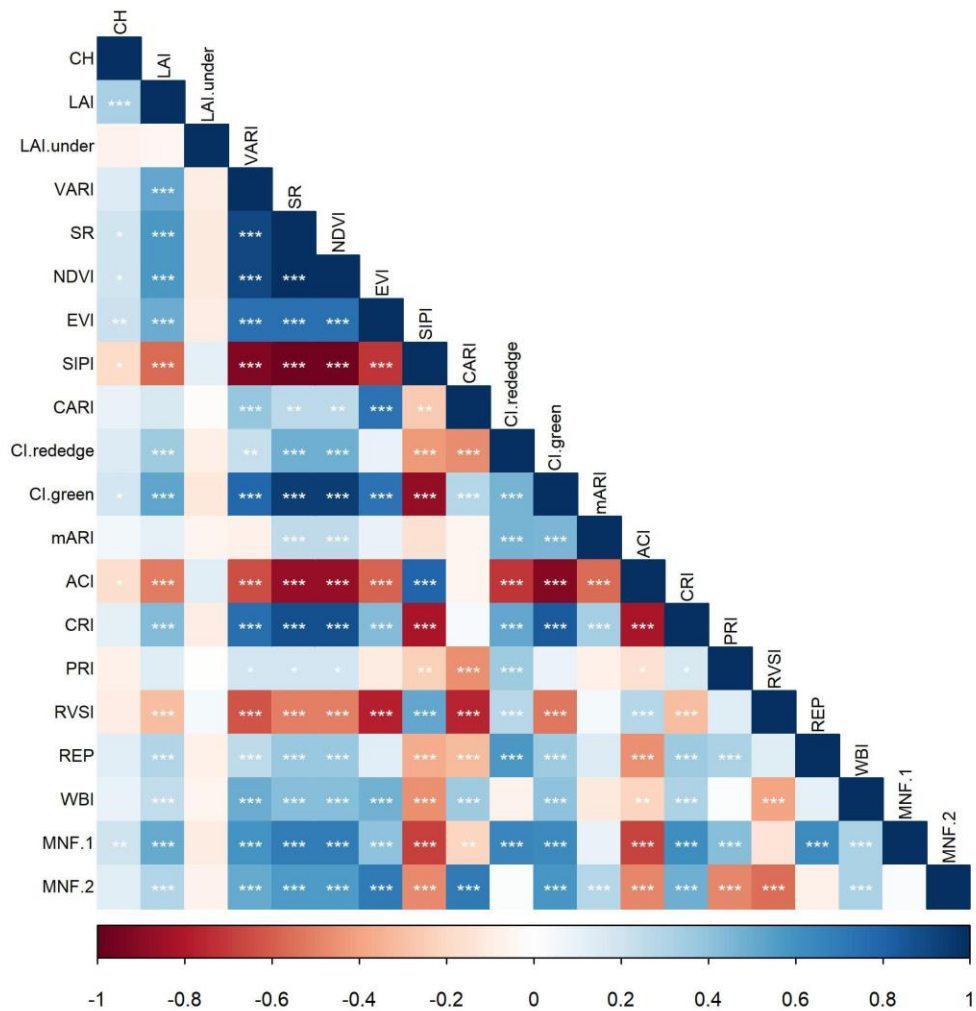
#### 371 **3.1. Variables derived from lidar and HSI**

372

373 Lidar-derived LAI was significantly correlated with almost all HSI-derived variables at  
374 the pixel level (Fig. 2). The structural VIs (HSI-derived) had the highest correlations with LAI  
375 ( $r > 0.50$ ,  $p$ -values  $< 0.05$ ). In general, structural VIs increased between LAI values ranging from  
376 0 to 2, but then saturated (Fig. 3). The canopy height attribute CH (lidar-derived) was  
377 significantly correlated with seven HSI-derived variables (Fig. 2), with EVI being the VI  
378 variable with the highest correlation ( $r = 0.22$ ,  $p$ -value = 0.006). The EVI and the other  
379 structural VIs all showed a positive correlation with CH for values ranging from 5 to 15 m, but  
380 they stabilized or decreased for CH values within 15-20 m (Fig. 3). The lidar-derived  
381 understory LAI (LAI.under) showed no significant correlation with any of the HSI-derived  
382 variables.

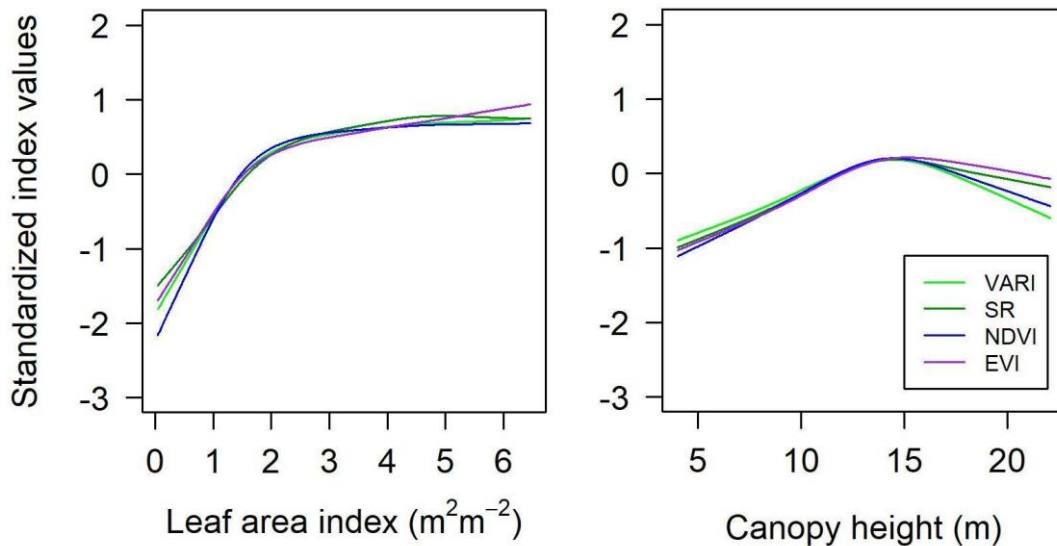
383

384



385  
 386 **Figure 2** - Spearman's correlation diagram among the lidar- and hyperspectral-derived  
 387 variables. The correlation values are ranked using a color gradient from -1 to 1, where 0 means  
 388 no correlation, -1 a strong negative correlation (red color), and one a strong positive correlation  
 389 (blue color). The *p*-value significance levels are "\*" 0.05, "\*\*\*" 0.01, and "\*\*\*\*" 0.001.  
 390 Acronyms of variables are described in Table 1.

391  
 392  
 393



394 **Figure 3** - Standardized hyperspectral-derived structural vegetation indices (Vegetation  
 395 Atmospherically Resistant Index - VARI, Simple Ratio - SR, Normalized Difference  
 396 Vegetation Index - NDVI, and Enhanced Vegetation Index - EVI) as a function of lidar-derived  
 397 leaf area index (LAI) (left) and lidar-derived canopy height (CH) (right). Lines are the  
 398 smoothed mean of the observations (pixels of 0.20 m resolution).  
 399

400  
 401

### 3.2. Distinguishing tree species richness levels

402  
 403  
 404

The 20 sp. treatment had lower field-derived AGB (mean  $\pm$  SE, 69.5  $\pm$  10.4 Mg/ha)  
 405 than the 60 sp. treatment (94.3  $\pm$  9.8 Mg/ha), whereas the 120 sp. treatment had intermediate  
 406 (88.7  $\pm$  15.6 Mg/ha) AGB and did not differ statistically from the other two treatments (Table  
 407 2). However, when changing the significance level to 0.1 (instead of 0.05), the two treatments  
 408 with the highest species richness (60 and 120 sp.) showed higher AGB than the treatment with  
 409 the lowest species richness (20 sp.).

The CH (lidar-derived) was higher in the two species-richer treatments (60 and 120 sp.)  
 410 (Table 2). However, the CH heterogeneity did not significantly differ between richness levels  
 411 (Table S1, p-value = 0.59). The richest treatment had the highest LAI value, and when  
 412 considering the significance level at 0.1, a significant increase in LAI was verified with the  
 413 increase in species richness class. The LAI heterogeneity was higher in the two richest  
 414 treatments (Table S1, p-value < 0.001). LAI<sub>under</sub> showed no difference among richness levels  
 415 (Table 2 and Fig. 5). The vertical distribution of the LAD was mono-modal, with a higher

417 concentration of vegetation in the middle layer of the canopy for all three treatments (Figure  
418 4).

419 For the HSI-derived VIs, the structural VIs (VARI, SR, NDVI, and EVI) increased with  
420 increasing richness (Table 2), and in some of them (VARI and NDVI), the heterogeneity was  
421 lower in the 120 sp. treatment (Table S1,  $p$ -values  $<0.05$ ). For the VIs related to chlorophyll  
422 concentration, SIPI decreased with increasing richness (SIPI is inversely proportional to  
423 chlorophyll concentration), while CI.rededge and CI.green increased with increasing species  
424 richness. The CARI VI showed no significant difference among richness treatments. For the  
425 VIs related to the anthocyanin concentration, the mARI has no significant difference, although  
426 its heterogeneity was greater in the richest treatment. ACI was lower in the lowest richness  
427 treatment. The VI related to carotenoid concentration, CRI, was higher in the richest treatment  
428 (with a significant gradual increase at the 0.1 significance level).

429 For the physiological VIs, RVSI decreased with the increase in richness, while the REP  
430 showed a directly proportional relationship with the increase in richness. WBI presented no  
431 significant difference, and PRI did not show a clear relationship with richness levels. The  
432 composition variable MNF.1 increased its mean and heterogeneity proportionally with richness  
433 (Table 2 and Table S1). The MNF.2 did not show any significant difference between  
434 treatments. Spectral variation increases with increasing richness (Fig. 5). The spectral angle, a  
435 proxy for the spectral diversity, showed a significant difference with richness levels only when  
436 the significance of 0.1 was considered ( $p$ -value = 0.09).

437  
438

439 **Table 2** - Statistical analysis (mean  $\pm$  SE; ANOVA *post hoc* Tukey) of field, lidar, and  
440 hyperspectral (HSI) variables by plot comparing diversity level treatments (20, 60, and 120  
441 sp.). Lidar and hyperspectral variables were summarized by the mean of the pixels (0.20 m  
442 resolution). The significant variables were colored green ranging from the lowest (light green)  
443 to the highest (dark green) values.

444

Type	Variable	Treatment			p-value
		20sp	60sp	120sp	
<b>Field</b>	AGB	69.459 ± 10.409 <b>b</b>	94.253 ± 9.736 <b>a</b>	88.698 ± 15.55 <b>ab</b>	0.043
<b>Lidar</b>	CH	10.331 ± 1.029 <b>b</b>	12.77 ± 1.098 <b>a</b>	12.993 ± 0.973 <b>a</b>	0.01
	LAI	1.063 ± 0.149 <b>b</b>	1.711 ± 0.139 <b>b</b>	2.639 ± 0.589 <b>a</b>	0.001
	LAI.under	0.074 ± 0.007	0.092 ± 0.017	0.08 ± 0.014	0.223
<b>Structural</b>	VARI	0.11 ± 0.023 <b>c</b>	0.167 ± 0.016 <b>b</b>	0.248 ± 0.003 <b>a</b>	< 0.001
	SR	7.728 ± 0.882 <b>c</b>	9.931 ± 0.94 <b>b</b>	12.987 ± 0.395 <b>a</b>	< 0.001
	NDVI	0.722 ± 0.024 <b>c</b>	0.776 ± 0.02 <b>b</b>	0.835 ± 0.007 <b>a</b>	< 0.001
	EVI	0.436 ± 0.009 <b>b</b>	0.496 ± 0.03 <b>ab</b>	0.534 ± 0.048 <b>a</b>	0.008
<b>Chlorophyll</b>	SIPI	1.118 ± 0.017 <b>a</b>	1.078 ± 0.012 <b>b</b>	1.042 ± 0.004 <b>c</b>	< 0.001
	CARI	0.027 ± 0.001	0.028 ± 0.002	0.027 ± 0.005	0.612
	CI.rededge	0.504 ± 0.038 <b>b</b>	0.556 ± 0.023 <b>ab</b>	0.622 ± 0.038 <b>a</b>	0.005
	CI.green	3.226 ± 0.179 <b>c</b>	3.719 ± 0.239 <b>b</b>	4.313 ± 0.082 <b>a</b>	< 0.001
<b>Anth/Caro</b>	mARI	1.691 ± 0.079	1.78 ± 0.143	1.798 ± 0.071	0.381
	ACI	0.193 ± 0.014 <b>a</b>	0.166 ± 0.011 <b>b</b>	0.143 ± 0.004 <b>b</b>	0.001
	CRI	12.574 ± 1.672 <b>b</b>	15.327 ± 1.834 <b>b</b>	19.802 ± 2.527 <b>a</b>	0.004
<b>Physiology</b>	PRI	-0.084 ± 0.002 <b>ab</b>	-0.086 ± 0.006 <b>b</b>	-0.071 ± 0.009 <b>a</b>	0.021
	RVSI	-0.009 ± 0.001 <b>a</b>	-0.01 ± 0.001 <b>ab</b>	-0.012 ± 0.001 <b>b</b>	0.032
	REP	715.857 ± 2.854 <b>b</b>	719.913 ± 2.389 <b>ab</b>	723.277 ± 2.091 <b>a</b>	0.014
	WBI	1.232 ± 0.014	1.233 ± 0.015	1.251 ± 0.008	0.169
<b>Hyperspectral variability</b>	MNF.1	-1.568 ± 0.431 <b>b</b>	-0.989 ± 0.187 <b>b</b>	1.125 ± 0.657 <b>a</b>	< 0.001
	MNF.2	-0.608 ± 0.322	0.118 ± 0.82	-0.079 ± 0.972	0.391
	Spectral angle	0.111 ± 0.008	0.122 ± 0.011	0.127 ± 0.004	0.09

446

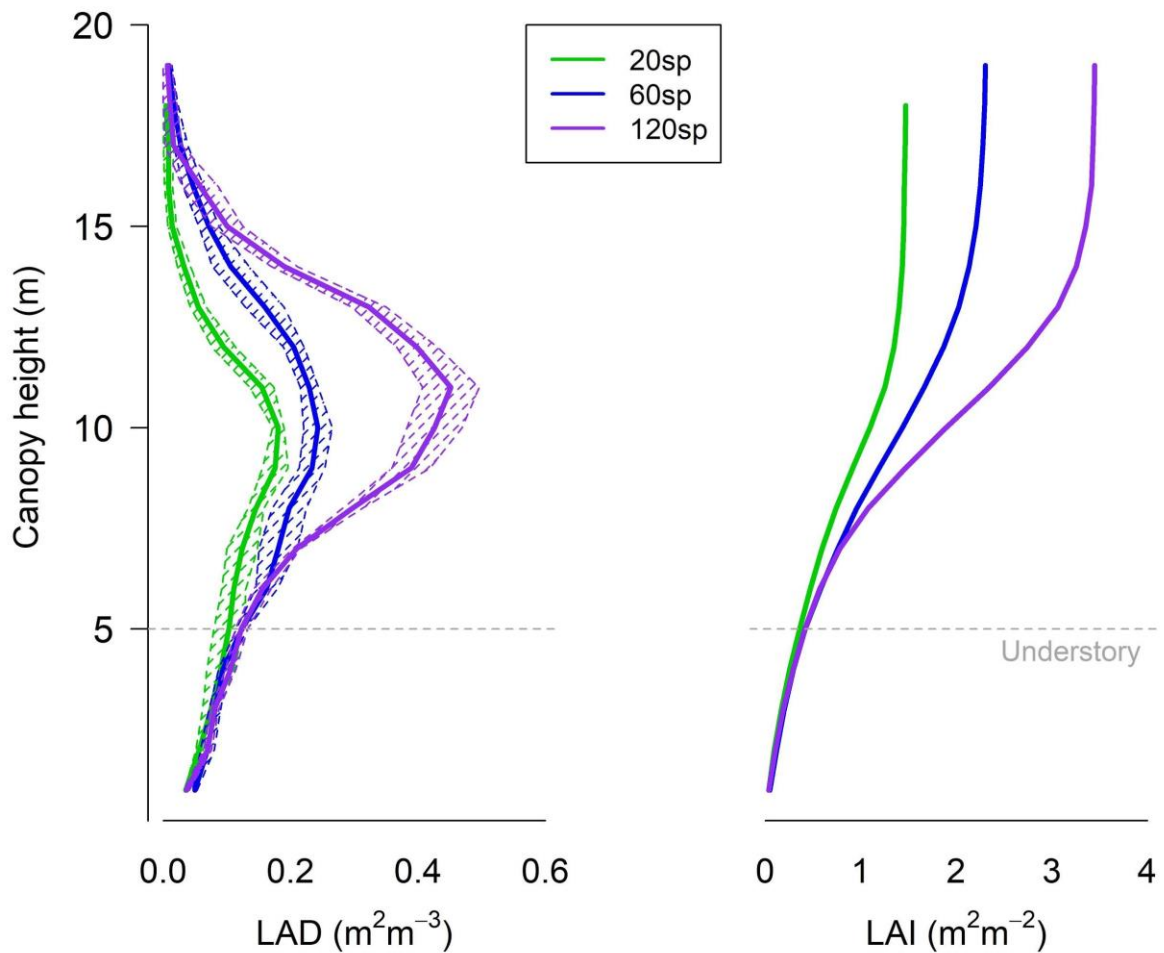
447

448

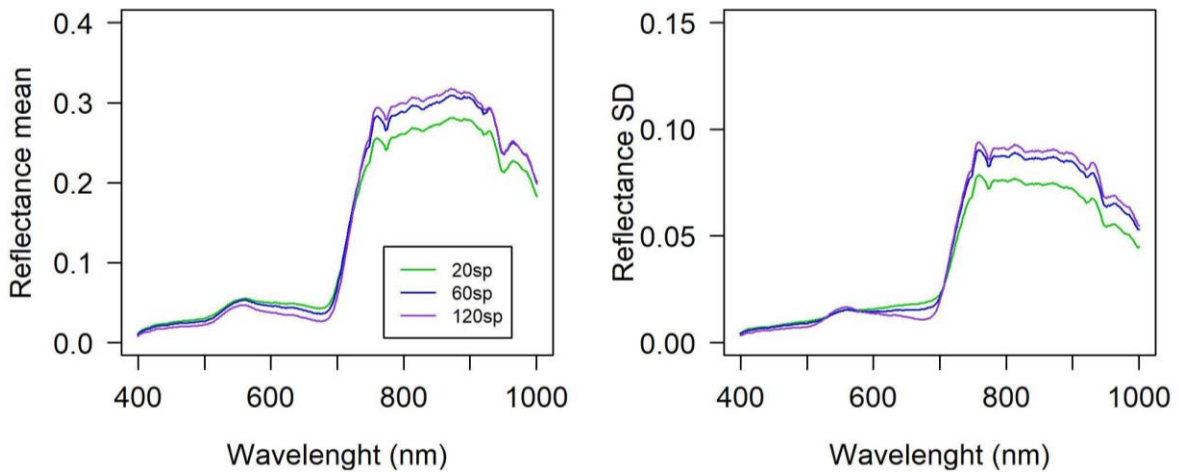
449

450

451



452 **Figure 4** - Mean leaf area density (LAD) profiles (left) and cumulative leaf area (LAI) (right)  
 453 for the three tree diversity level treatments (20, 60, and 120 sp.). Lines are the plots' mean, and  
 454 the dashed polygons represent the standard error amplitude.  
 455  
 456  
 457

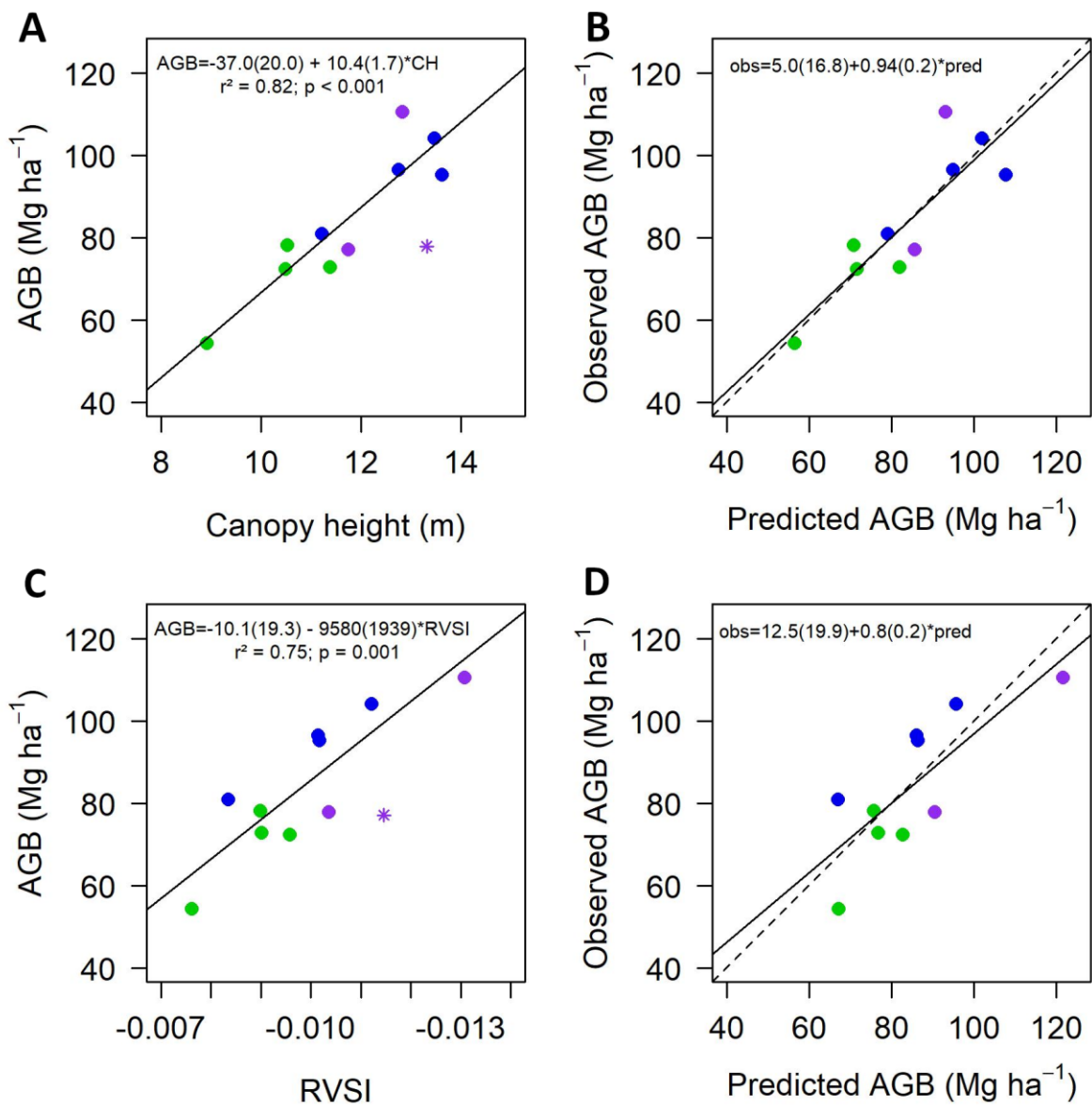


458 **Figure 5** - Mean (left) and standard deviation (SD) (right) of reflectance for the three tree  
 459 richness level treatments (20, 60, and 120 sp.).  
 460  
 461

462  
463  
464  
465  
466  
467  
468  
469  
470  
471  
472

### 3.3. Predicting aboveground biomass

The AGB were significantly correlated ( $p < 0.001$ ) with one lidar-derived variable (CH,  $r^2 = 0.81$ ), and three HIS-derived VIs (RVSI,  $r^2 = 0.78$ ; EVI,  $r^2 = 0.76$ ; and CARI,  $r^2 = 0.77$ ) (Figure S2). However, after eliminating an outlier observation, the best AGB predictors were CH ( $r^2 = 0.82$ , RMSE = 7.62, relative RMSE = 9.0%), followed by the RVSI ( $r^2 = 0.75$ , RMSE = 8.98, relative RMSE = 10.1%) (Figure 6). Multiple regression models did not provide significant improvements.



473

474 **Figure 6** - Aboveground biomass of plots as a function of (A) lidar-derived canopy height  
475 (CH); and (C) hyperspectral-derived RVSI. The “\*” purple point is an outlier plot not included  
476 in these regressions. Numbers in parentheses are the standard errors for each coefficient. (B)  
477 and (D) are Leave-one-out cross-validations (LOOCV) of aboveground biomass as a function  
478 of CH and RVSI, respectively. The dashed line represents a 1:1 correspondence, and the solid  
479 line is the linear regression fit between observed and leave-one-out predicted values ( $obs_i = \alpha$   
480  $+ \beta \cdot pred_i$ ). The values of  $\alpha$  and  $\beta$  showed no significant difference from 0 and 1, respectively,  
481 in both cases. Point color represents the treatments of 20, 60, and 120 species (green, blue and  
482 purple, respectively).

483  
484

#### 485 **4. DISCUSSION**

486  
487

Our UAV-lidar-HSI system showed a strong potential to assess canopy structure, AGB,  
488 and tree diversity in tropical forest restoration plots, combining lidar and the VIs derived from  
489 HSI. It also helped reveal a suite of canopy differences related to forest structure and ecosystem  
490 function over an experimental biodiversity gradient. This included both bulk properties like  
491 height and LAI (from lidar) and physiologically-linked community traits such as EVI  
492 ‘greenness’ (from hyperspectral), consistent with theories about the advantages of higher  
493 biodiversity in restoration. To our knowledge, this is the first study to use both lidar and HSI  
494 onboard a UAV to monitor tropical forest restoration (but see Vaglio Laurin et al. 2014 for a  
495 pioneer attempt in a mature tropical forest).

496  
497

##### 497 **4.1. Variables derived from lidar and HSI**

498  
499

Almost all HSI variables were significantly correlated with the LAI. In general, VIs  
500 including information from the NIR domain (750-850 nm, a spectral region characterized by  
501 multiple scattering of foliar tissues) show sensitivity to LAI. However, the VIs tend to saturate  
502 for LAI values higher than 2. Only mARI and PRI (which do not use NIR information) did not  
503 correlate with LAI. VARI and CRI do not have NIR bands in their equation but nonetheless  
504 showed a saturating correlation with LAI. These VIs are related to the photosynthetically active  
505 leaf area, with VARI using the ratios between the green (~ 550 nm) and red (~ 650 nm) bands  
506 and the CRI using two different green bands (~ 500nm) (Gitelson et al. 2002 and 2007). VARI

507 has been proposed as a substitute for NDVI to measure canopy structure using ordinary RGB  
508 images (Fuentes-Peailillo et al. 2018; Gitelson et al. 2002). Among the structural VIs, EVI is  
509 known to have lesser degree of saturation with increasing LAI due to its higher sensitivity to  
510 NIR reflectance (non-saturated) than red reflectance, making it more responsive to canopy  
511 structural variations than indices such as NDVI (e.g. Huete et al. 2002). However, in our study  
512 EVI showed saturation at LAI=2.0. Our analysis was conducted on an unprecedented fine  
513 spatial scale, allowing a better understanding of the relationship between the LAI and the VIs  
514 derived from high-spatial-resolution optical sensors, without the confounding effects of leaf  
515 age or sub-pixel shade fraction. Nevertheless, relationships (including VIs saturation) may be  
516 dependent on season and spatial resolution, an important question for future UAV-based high-  
517 resolution analysis that must be answered to connect UAV observations to those from coarser  
518 grain airborne and orbital sensors. We also note that the lidar-derived LAI represents a proxy  
519 for the actual LAI (Almeida et al. 2019c) and includes surface area contributions from other  
520 canopy components such as branches.

521 As expected, no HSI-derived variable was correlated to the understory LAI since HSI  
522 data are limited to the canopy surface, as is usual for optical sensors. On the other hand, lidar  
523 can record understory vegetation, providing information for forest restoration monitoring. The  
524 understory LAI showed potential to distinguish forest succession stages and forest types  
525 (Almeida et al. 2019a and 2020). Almeida et al. (2020), using a UAV-lidar system, showed  
526 that forest age was negatively correlated with understory LAI.

527 Some structural VIs were less spatially heterogeneous in the plots with higher LAI  
528 values (and higher richness levels). The saturation effect, in those cases, decreased their spatial  
529 heterogeneity, limiting the effectiveness of methods based on the spatial variation of VIs for  
530 estimating tree species diversity or the separation of forest types. VIs are limited in  
531 distinguishing between secondary and primary growth forests. However, using multiangular,

532 off-nadir viewing hyperspectral data can improve forest successional stage discrimination  
533 (Galvão et al. 2009; Garcia Millan and Sanchez-Azofeifa 2018). Combining temporal VIs  
534 analyses of land cover (vegetation or exposed soil) allows the determination of cover classes  
535 such as forest regeneration (including forest age) or short-term agricultural crop (Silva Junior  
536 et al. 2020).

537         The restoration plantations that we studied have a more homogenous canopy structure  
538 when compared with sites under natural regeneration, likely related to the even-aged cohort  
539 that comprises the canopy layer. We expect heterogeneity to increase with time through stand  
540 development competitive thinning dynamics, enhanced potentially by the years-to-decades that  
541 some slow-growing tropical trees require to express their unique structural characteristics and  
542 profile in the canopy. We believe that the ability of lidar technology to differentiate tree  
543 diversity levels may improve along with the structural development of forest stands.  
544 Conversely, the HSI spatial patterns were relevant proxies for distinguishing tree diversity  
545 levels even in 13-year-old restoration, highlighting the potential of this technology to monitor  
546 broad-scale restoration programs.

#### 547                   **4.2. Distinguishing tree species richness levels**

549         Several lidar-derived variables were more sensitive to differences in diversity than  
550 AGB. While we detected differences in AGB only between the treatments with 20 and 60 sp.,  
551 LAI differed among all three diversity treatments and increased with each increasing species  
552 richness level. For the same study site, Duarte et al. (2021) found that AGB saturated from 60  
553 sp. to 120 sp. while LAI and light interception (both derived from LAI-2200C equipment) were  
554 positively correlated to diversity even at very high richness levels. However, both our and  
555 Duarte et al. study evaluated only stem AGB and did not consider branches and leaves. Our  
556 results also showed that canopy height was positively associated with species richness.  
557 Previous studies have shown that enhanced light interception and LAI in diverse tropical forests  
558

559 result from enhanced complementarity among crowns in canopy space, promoted by a high  
560 diversity of crown shapes and heights among species and neighborhood-driven plasticity in  
561 crowns (Guillemot et al. 2020, Duarte et al. 2021, Williams et al. 2017). We showed that the  
562 diversity effects on stand structure and AGB were efficiently captured by lidar-derived  
563 variables, which open promising perspectives for the large-scale monitoring of hyper-diverse  
564 tropical forest functioning. Canopy height heterogeneity and the LAI under the canopy did not  
565 significantly vary among treatments, which may be explained by the forest's low maturity and  
566 structural homogeneity. Increasing diversity and associated LAI in the upper canopy do not  
567 appear to impact understory LAI. A potential explanation for this surprising result is that light  
568 use efficiency increases with diversity—an expectation of higher crown type diversity—such  
569 that understory light availability changes little over this diversity gradient.

570         Structural VIs were positively associated with species richness. The capacity of VIs to  
571 discriminate among richness levels can be explained by the relatively low LAI compared with  
572 natural regeneration and mature forests (Almeida et al. 2019a). However, increasing LAI may  
573 result in saturation of the structural VIs and reduced ability to differentiate among richness  
574 levels. In general, the VIs that showed a significant difference among the treatments also  
575 showed an association with the canopy structure (i.e., significant correlation with LAI). It is  
576 important to note that many of the biochemical VIs were developed from laboratory  
577 spectrometers characterized by a higher signal-to-noise ratio (Meneses et al. 2019). The aerial  
578 collection of hyperspectral images (e.g. from drones) is subject to interference from the  
579 conditions of acquisition (atmospheric properties, geometry of acquisition) and canopy  
580 structure. However, some studies have shown promising results from VIs for tropical tree  
581 species classification (Ferreira et al. 2016).

582         One of the most interesting results concerning HSI data was that spectral diversity  
583 appeared to increase with richness treatments. The spectral angle was significantly different

584 across categorical classes of species richness at  $p < 0.1$  (Tukey test) and at  $p < 0.05$  when  
585 species richness was treated as a continuous predictor in a simple linear regression (Table S2).  
586 The hyperspectral composition variable (MNF.1) differed among treatments in both mean and  
587 variance, and the spectral response showed higher variability in treatments with greater  
588 diversity (Fig. 5). By computing the spectral angle among the treatments, we showed that the  
589 spectral variability increased with diversity, which broadly agrees with the spectral variation  
590 hypothesis (Palmer et al. 2002). This hypothesis states that the spectral heterogeneity is induced  
591 by variations in habitat and has been used to assess forest canopy diversity with hyperspectral  
592 data (Féret and Asner, 2014). Our results suggested that tree diversity itself impacts spectral  
593 heterogeneity.

594  
595

### 596 **4.3. Predicting aboveground biomass**

597  
598 Some lidar and HSI variables demonstrated a remarkable capacity to estimate AGB  
599 accurately. This prediction represents a well-known potential of lidar structural data but is a  
600 less-universal finding for HSI variables. While VIs are known to saturate at high biomass and  
601 LAI values, the low plot-level density of vegetation (LAI  $\sim 2$ ) in our study maintained VIs in  
602 an unsaturated range, where there is a strong correlation with AGB. This non-saturated stage  
603 behavior was also found in another study focusing on young, low diversity plantations  
604 established in a temperate forest ecosystem (Williams et al. 2021). The RVSI (Red-edge  
605 Vegetation Stress Index) was the most accurate predictor for biomass, which can be explained  
606 by the high positive correlation between the red-edge region (680–750 nm), the chlorophyll  
607 content, and the canopy LAI (Fillela & Penuelas, 1994). The increase in the chlorophyll content  
608 tends to move the red-edge position to longer wavelengths, while the increase in LAI increases  
609 the difference between NIR and red reflectance. As the RVSI uses bands near the end of the

610 red edge (>730 nm), it may be sensitive to AGB variations induced by LAI and chlorophyll  
611 content.

612 The AGB predictions performed by the structural attribute derived from lidar (canopy  
613 height) did better than that of HSI-derived VIs. Lidar sensors have been shown to be the best  
614 tool for AGB estimates, especially in dense tropical rainforests (Wulder et al. 2012). Adding  
615 more variables to the model (multiple regression models) did not improve the prediction,  
616 probably due to the low structural complexity and low age of the vegetation. In a previous  
617 study performed in the same region but based on a greater number of forest types and more  
618 structurally complex forests, the addition of more variables improved AGB models (Almeida  
619 et al. 2019a). The utility of fusing lidar and hyperspectral data for AGB prediction *per se*  
620 remains an unresolved problem in the literature. Some studies have shown slight improvement  
621 with the addition of hyperspectral metrics in the AGB estimation models when they already  
622 have included lidar metrics (e.g. Clark et al. 2011; Fassnacht et al. 2014), while others have  
623 found better performance mixing lidar and HSI variables (e.g. de Almeida et al. 2019; Vaglio  
624 Laurin et al. 2014).

625 The use of lidar data as an intermediary layer between field and spectral satellite data  
626 (“upscaling” technique) is critical to generate large samples of AGB with high accuracy and  
627 thus generate more robust maps using satellite images for more extensive areas. Csillik et al.  
628 (2019) combined lidar and high-resolution satellite images to generate a biomass map for the  
629 entire country of Peru. New orbital lidar sensors are expected to generate more accurate maps  
630 of tropical forest AGB and stand structure attributes. One of them is the “Global Ecosystem  
631 Dynamics Investigation” (GEDI) orbital lidar sensor; however, its information is not spatially  
632 continuous and has much lower precision and accuracy compared with lidar sensors onboard  
633 aircraft and UAVs (Dubayah et al. 2020).

634  
635

#### **4.4. Monitoring tropical forest restoration**

636  
637           Given the high cost of field inventories, restoration programs have often used an  
638 insufficient number of plots, which have ultimately compromised the reliability of restoration  
639 field assessments (Viani et al. 2018). Upscaling restoration monitoring requires more than the  
640 replication over space of traditional forest inventory approaches because of the costs and scales  
641 involved (Brancalion et al. 2017). At the other extreme, satellite images and novel analytical  
642 approaches are still incapable of measuring restoration quality (Rosa et al. 2021). A successful  
643 monitoring program must consider the gap between detailed and costly information from field  
644 plots and the million hectares of information generated by satellites with low capacity to detect  
645 restoration success.

646           We believe that the novel UAV-borne lidar and hyperspectral system described here  
647 can fill this technological gap, offering data streams that can be connected with plot-based  
648 monitoring and broad-scale remote sensing alike to improve upscaling and forest restoration  
649 monitoring. Particularly by blending lidar and HSI data, it is possible to assess biomass  
650 structural, functional, and diversity linked restoration outcomes simultaneously, a great  
651 advantage over methods based solely on either lidar or HSI. Further, it may represent a  
652 revolution in tracking restoration success globally. The development of new remote sensing  
653 approaches and their application to a restoration context would help expand our capacity to  
654 assess restoration over unprecedented spatial and temporal scales (White et al. 2019). Lidar-  
655 HSI upscaling has recently become possible due to the new generation of orbital sensors. In  
656 addition to the abovementioned spaceborne GEDI lidar mission, the DESIS (Krutz et al., 2019)  
657 and PRISMA (Vangi et al., 2019) hyperspectral sensors provide data with fine sampling using  
658 narrow bands (lower than 10 nm) and 30 m of spatial resolution. Together GEDI and DESIS  
659 or PRISMA data can provide unprecedented results on the structure and diversity of forest  
660 restoration at broader spatial scales. UAV-lidar-HSI systems are still relatively expensive and

661 potentially unaffordable by some decision-making organizations such as governments, NGOs,  
662 small landowners, and companies.

663 In addition to acquisition costs, a high level of technical knowledge is required to  
664 operate drone-based systems and process and analyze the data. Thus, their use is still  
665 constrained to a minority of research groups. In tropical countries, particularly, the use of these  
666 systems is considerably limited due to high import tariffs and a lack of local technical  
667 assistance. However, these initial constraints are precisely the same faced by other  
668 technological innovations of the past, which are now broadly present in modern societies  
669 worldwide. Despite the constraints, efficient and relatively inexpensive UAV-lidar systems  
670 have been developed (Hu et al. 2021), which may facilitate their broader use in diverse sectors,  
671 particularly in forest restoration. Institutions in tropical countries should encourage the  
672 development of these technologies through investing in research, eliminating import taxes,  
673 encouraging open hardware development (Tsanni 2020) and facilitating the arrival of  
674 specialized companies.

675 There are many benefits that UAV-lidar-HSI systems bring to forest restoration  
676 monitoring, including the potential to monitor small areas with very high accuracy, reduced  
677 field sampling effort (Papa et al. 2020), and the increase of remote sampling for upscaling and  
678 generation of global models. Standardized monitoring protocols would help to evaluate  
679 restoration strategies' efficacy and compare results across projects to learn from the past and  
680 inform future restoration efforts (Viani et al. 2017). The unprecedented scale of global forest  
681 restoration targets will need to be accompanied by the evolution of restoration monitoring  
682 approaches and delivering, at much-reduced costs and higher spatial and temporal scales,  
683 critical information for tracking restoration success and guiding adaptive management. This  
684 constitutes an enormous scientific and technological challenge that has just started to be  
685 addressed by a joint effort of restoration, policymakers, and remote sensing experts. The

686 positive results obtained by the UAV-lidar-HSI system described here are very encouraging  
687 and may hopefully foster the ongoing development and application of remote sensing  
688 innovations in ecosystem restoration.

689

## 690 ACKNOWLEDGMENTS

691 The São Paulo Research Foundation (FAPESP, grants #2018/21338-3, #2018/18416-2,  
692 #2019/14697-0, #2019/08533-4 and #2019/24049-5) is acknowledged for financial support.  
693 We thank the McIntire-Stennis program of the USDA for support towards the GatorEye system  
694 development. P. Meli is supported by Fondecyt (project 11191021). M.P. Ferreira was  
695 supported by the Brazilian National Council for Scientific and Technological Development  
696 (CNPq) (grant #306345/2020-0). A.P.D. Corte was supported by the Brazilian National  
697 Council for Scientific and Technological Development (CNPq) (#302891/2018-8;  
698 #408785/2018-7). SC Stark was supported by National Science Foundation (NSF) DEB-  
699 1754357, DEB-1950080, EF-1340604, and EF-1550686. J.-B. Féret acknowledges financial  
700 support from Agence Nationale de la Recherche (BioCop project—ANR-17-CE32-0001).

701

702

703

## 704 REFERENCES

705

706 Adhikari, H., Valbuena, R., Pellikka, P.K.E. & Heiskanen, J. (2020). Mapping forest  
707 structural heterogeneity of tropical montane forest remnants from airborne laser scanning  
708 and Landsat time series. *Ecological Indicators*, **108**, 105739.

709 Ali, A., Lin, S.-L., He, J.-K., Kong, F.-M., Yu, J.-H. & Jiang, H.-S. (2019). Climate and soils  
710 determine aboveground biomass indirectly via species diversity and stand structural  
711 complexity in tropical forests. *Forest Ecology and Management*, **432**, 823–831.

712 Almeida, D.R.A., Almeyda Zambrano, A.M., Broadbent, E.N., Wendt, A.L., Foster, P.,  
713 Wilkinson, B.E., Salk, C., Papa, D. de A., Stark, S.C., Valbuena, R., Gorgens, E.B.,  
714 Silva, C.A., Brancalion, P.H.S., Fagan, M., Meli, P. & Chazdon, R. (2020). Detecting  
715 successional changes in tropical forest structure using GatorEye drone-borne lidar.  
716 *Biotropica*, **52**, 1155–1167.

717 Almeida, D.R.A., Stark, S.C., Valbuena, R., Broadbent, E.N., Silva, T.S.F., Resende, A.F.,  
718 Ferreira, M.P., Cardil, A., Silva, C.A., Amazonas, N., Zambrano, A.M.A. & Brancalion,  
719 P.H.S. (2020b). A new era in forest restoration monitoring. *Restoration Ecology*.

720 Almeida, D.R.A., Stark, S.C., Chazdon, R., Nelson, B.W., Cesar, R.G., Meli, P., Gorgens,  
721 E.B., Duarte, M.M., Valbuena, R., Moreno, V.S., Mendes, A.F., Amazonas, N.,  
722 Gonçalves, N.B., Silva, C.A., Schiatti, J. & Brancalion, P.H.S. (2019a). The  
723 effectiveness of lidar remote sensing for monitoring forest cover attributes and landscape  
724 restoration. *Forest Ecology and Management*, **438**, 34–43.

725 Almeida, D.R.A., Broadbent, E.N., Zambrano, A.M.A., Wilkinson, B.E., Ferreira, M.E.,

- 726 Chazdon, R., Meli, P., Gorgens, E.B., Silva, C.A., Stark, S.C., Valbuena, R., Papa, D.A.  
727 & Brancalion, P.H.S. (2019b). Monitoring the structure of forest restoration plantations  
728 with a drone-lidar system. *International Journal of Applied Earth Observation and*  
729 *Geoinformation*, **79**, 192–198.
- 730 Almeida, D.R.A. de, Stark, S.C., Shao, G., Schietti, J., Nelson, B.W., Silva, C.A., Gorgens,  
731 E.B., Valbuena, R., Papa, D. de A. & Brancalion, P.H.S. (2019c). Optimizing the  
732 Remote Detection of Tropical Rainforest Structure with Airborne Lidar: Leaf Area  
733 Profile Sensitivity to Pulse Density and Spatial Sampling. *Remote sensing*, **11**, 92.
- 734 Almeida, D. R. A.; Stark, S.C; Silva, C. A.; Hamamura, C. and Valbuena, R. (2019d). leafR:  
735 Calculates the Leaf Area Index (LAI) and Other Related Functions. R package version  
736 0.3. <https://CRAN.R-project.org/package=leafR>
- 737 Amaral, C.H. do, Almeida, T.I.R. de, Souza Filho, C.R. de, Roberts, D.A., Fraser, S.J., Alves,  
738 M.N. & Botelho, M. (2018). Characterization of indicator tree species in neotropical  
739 environments and implications for geological mapping. *Remote Sensing of Environment*,  
740 **216**, 385–400.
- 741 Asner, G.P., Martin, R.E., Knapp, D.E., Tupayachi, R., Anderson, C.B., Sinca, F., Vaughn,  
742 N.R., Llactayo, W., 2017. Airborne laser-guided imaging spectroscopy to map forest trait  
743 diversity and guide conservation. *Science* 355, 385–389. Asner, G.P. (2015). Organismic  
744 remote sensing for tropical forest ecology and conservation<sup>1, 2</sup>. *Annals of the Missouri*  
745 *Botanical Garden*, **100**, 127–140.
- 746 Asner, G.P. & Martin, R.E. (2009). Airborne spectranomics: mapping canopy chemical and  
747 taxonomic diversity in tropical forests. *Frontiers in Ecology and the Environment*, **7**,  
748 269–276.
- 749 Brancalion, P.H.S. & Holl, K.D. (2020). Guidance for successful tree planting initiatives.  
750 *Journal of Applied Ecology*.
- 751 Brancalion, P.H.S. & van Melis, J. (2017). On the need for innovation in ecological  
752 restoration. *Annals of the Missouri Botanical Garden*, **102**, 227–236.
- 753 Broadbent, E.N.; Zambrano, A.M.A.; Omans, G.; Adler, A.; Alonso, P.; Naylor, D.;  
754 Chenevert, G.; Murtha, T.; Vogel, J.; Almeida, D.R.A.; Dalla Corte, A.P.; Silva, C.A.;  
755 Prata, G.A.; Merrick, T.; D'Oliveira, M.V.N.; Detto, M.; Ferreira, M.P.; Wilkinson,  
756 B.E.; Ferreira, M.E.; Landau, H. M. (*in prep*). The GatorEye Unmanned Flying  
757 Laboratory: sensor fusion for 4D ecological analysis through custom hardware and  
758 algorithm integration. <http://www.speclab.org/gatoreye.html> (Accessed 08 June 2021).
- 759 Camarretta, N., Harrison, P.A., Bailey, T., Potts, B., Lucieer, A., Davidson, N. & Hunt, M.  
760 (2020). Monitoring forest structure to guide adaptive management of forest restoration: a  
761 review of remote sensing approaches. *New Forests*, **51**, 573–596.
- 762 Chagas, G., Salk, C.F., Vidal, E.J., Souza, S.E.X.F. & Brancalion, P.H.S. (2021). Exploiting  
763 fruits of a threatened palm to trigger restoration of Brazil's Atlantic Forest. *Restoration*  
764 *Ecology*, **29**.
- 765 Clark, M.L., Roberts, D.A., Ewel, J.J. & Clark, D.B. (2011). Estimation of tropical rain forest

766 aboveground biomass with small-footprint lidar and hyperspectral sensors. *Remote*  
767 *Sensing of Environment*, **115**, 2931–2942.

768 Crouzeilles, R., Santiami, E., Rosa, M., Pugliese, L., Brancalion, P.H.S., Rodrigues, R.R.,  
769 Metzger, J.P., Calmon, M., Scaramuzza, C.A. de M., Matsumoto, M.H., Padovezi, A.,  
770 Benini, R. de M., Chaves, R.B., Metzker, T., Fernandes, R.B., Scarano, F.R., Schmitt, J.,  
771 Lui, G., Christ, P., Vieira, R.M. & Pinto, S. (2019). There is hope for achieving  
772 ambitious Atlantic Forest restoration commitments. *Perspectives in Ecology and*  
773 *Conservation*, **17**, 80–83.

774 da Costa, V.A.M., de Oliveira, A. da F., dos Santos, J.G., Bovo, A.A.A., de Almeida, D.R.A.  
775 & Gorgens, E.B. (2020). Assessing the utility of airborne laser scanning derived  
776 indicators for tropical forest management. *Southern Forests: a Journal of Forest Science*,  
777 **82**, 352–358.

778 Dalagnol, R., Wagner, F.H., Galvão, L.S., Streher, A.S., Phillips, O.L., Gloor, E., Pugh,  
779 T.A.M., Ometto, J.P.H.B. & Aragão, L.E.O.C. (2021). Large-scale variations in the  
780 dynamics of Amazon forest canopy gaps from airborne lidar data and opportunities for  
781 tree mortality estimates. *Scientific Reports*, **11**, 1388.

782 Dalla Corte, A.P., Rex, F.E., Almeida, D.R.A. de, Sanquetta, C.R., Silva, C.A., Moura, M.M.,  
783 Wilkinson, B., Zambrano, A.M.A., Cunha Neto, E.M. da, Veras, H.F.P., Moraes, A. de,  
784 Klauberg, C., Mohan, M., Cardil, A. & Broadbent, E.N. (2020). Measuring Individual  
785 Tree Diameter and Height Using GatorEye High-Density UAV-Lidar in an Integrated  
786 Crop-Livestock-Forest System. *Remote sensing*, **12**, 863.

787 de Almeida, C.T. de, Galvão, L.S., Aragão, L.E. de O.C. e, Ometto, J.P.H.B., Jacon, A.D.,  
788 Pereira, F.R. de S., Sato, L.Y., Lopes, A.P., Graça, P.M.L. de A., Silva, C.V. de J.,  
789 Ferreira-Ferreira, J. & Longo, M. (2019). Combining LiDAR and hyperspectral data for  
790 aboveground biomass modeling in the Brazilian Amazon using different regression  
791 algorithms. *Remote Sensing of Environment*, **232**, 111323.

792 De Cáceres, M., Martín-Alcón, S., González-Olabarria, J.R. & Coll, L. (2019). A general  
793 method for the classification of forest stands using species composition and vertical and  
794 horizontal structure. *Annals of forest science*, **76**, 40.

795 Dickinson, Y., Pelz, K., Giles, E. & Howie, J. (2016). Have we been successful? Monitoring  
796 horizontal forest complexity for forest restoration projects. *Restoration Ecology*, **24**, 8–  
797 17.

798 d'Oliveira, M.V.N., Broadbent, E.N., Oliveira, L.C., Almeida, D.R.A., Papa, D.A., Ferreira,  
799 M.E., Zambrano, A.M.A., Silva, C.A., Avino, F.S., Prata, G.A., Mello, R.A., Figueiredo,  
800 E.O., Jorge, L.A. de C., Junior, L., Albuquerque, R.W., Brancalion, P.H.S., Wilkinson,  
801 B. & Oliveira-da-Costa, M. (2020). Aboveground Biomass Estimation in Amazonian  
802 Tropical Forests: a Comparison of Aircraft- and GatorEye UAV-borne LiDAR Data in  
803 the Chico Mendes Extractive Reserve in Acre, Brazil. *Remote sensing*, **12**, 1754.

804 Duarte, M. M., Moral, R. A., Guillemot, J., Isaac, C., Zuim, F., Potvin, C., Bonat, W. H.,  
805 Stape, J. L., Brancalion, P. H. S. (2021). High tree diversity enhances light interception

806 in tropical forests. *Journal of Ecology*

807 Dubayah, R., Blair, J.B., Goetz, S., Fatoyinbo, L., Hansen, M., Healey, S., Hofton, M., Hurtt,  
808 G., Kellner, J., Luthcke, S., Armston, J., Tang, H., Duncanson, L., Hancock, S., Jantz, P.,  
809 Marselis, S., Patterson, P.L., Qi, W. & Silva, C. (2020). The Global Ecosystem  
810 Dynamics Investigation: High-resolution laser ranging of the Earth's forests and  
811 topography. *Science of Remote Sensing*, **1**, 100002.

812 Erbaugh, J.T. & Oldekop, J.A. (2018). Forest landscape restoration for livelihoods and well-  
813 being. *Current Opinion in Environmental Sustainability*, **32**, 76–83.

814 Fagan, M.E., Reid, J.L., Holland, M.B., Drew, J.G. & Zahawi, R.A. (2020). How feasible are  
815 global forest restoration commitments? *Conservation letters*.

816 Fassnacht, F.E., Hartig, F., Latifi, H., Berger, C., Hernández, J., Corvalán, P. & Koch, B.  
817 (2014). Importance of sample size, data type and prediction method for remote sensing-  
818 based estimations of aboveground forest biomass. *Remote Sensing of Environment*, **154**,  
819 102–114.

820 Feret, J.-B. & Asner, G.P. (2013). Tree species discrimination in tropical forests using  
821 airborne imaging spectroscopy. *IEEE Transactions on Geoscience and Remote Sensing*,  
822 **51**, 73–84.

823 Féret, J.-B. & Asner, G.P. (2014). Mapping tropical forest canopy diversity using high-  
824 fidelity imaging spectroscopy. *Ecological Applications*, **24**, 1289–1296.

825 Ferez, A.P., 2012. Efeito de práticas silviculturais sobre as taxas iniciais de sequestro de  
826 carbono em plantios de restauração da Mata Atlântica. Master thesis, Universidade de  
827 São Paulo, Piracicaba, São Paulo, Brazil. p. 104.

828 Ferez, A.P.C., Campoe, O.C., Mendes, J.C.T. & Stape, J.L. (2015). Silvicultural opportunities  
829 for increasing carbon stock in restoration of Atlantic forests in Brazil. *Forest Ecology*  
830 *and Management*, **350**, 40–45.

831 Ferreira, M.P., Almeida, D.R.A. de, Papa, D. de A., Minervino, J.B.S., Veras, H.F.P.,  
832 Formighieri, A., Santos, C.A.N., Ferreira, M.A.D., Figueiredo, E.O. & Ferreira, E.J.L.  
833 (2020). Individual tree detection and species classification of Amazonian palms using  
834 UAV images and deep learning. *Forest Ecology and Management*, **475**, 118397.

835 Ferreira, M.P., Féret, J.-B., Grau, E., Gastellu-Etchegorry, J.-P., Shimabukuro, Y.E. & de  
836 Souza Filho, C.R. (2018). Retrieving structural and chemical properties of individual tree  
837 crowns in a highly diverse tropical forest with 3D radiative transfer modeling and  
838 imaging spectroscopy. *Remote Sensing of Environment*, **211**, 276–291.

839 Ferreira, M.P., Wagner, F.H., Aragão, L.E.O.C., Shimabukuro, Y.E. & de Souza Filho, C.R.  
840 (2019). Tree species classification in tropical forests using visible to shortwave infrared  
841 WorldView-3 images and texture analysis. *ISPRS Journal of Photogrammetry and*  
842 *Remote Sensing*, **149**, 119–131.

843 Ferreira, M.P., Zortea, M., Zanotta, D.C., Shimabukuro, Y.E. & de Souza Filho, C.R. (2016).  
844 Mapping tree species in tropical seasonal semi-deciduous forests with hyperspectral and

845 multispectral data. *Remote Sensing of Environment*, **179**, 66–78.

846 Fox, J., & Weisberg, S. (2019). *An R Companion to Applied Regression* (3<sup>rd</sup> ed.). Thousand  
847 Oaks CA: Sage. Retrieved from [https://socialsciences.mcmaster.ca/jfox/Books/Companion/Filella, I. & Penuelas, J. \(1994\). The red edge position and shape as indicators of plant chlorophyll content, biomass and hydric status. International journal of remote sensing, 15, 1459–1470.](https://socialsciences.mcmaster.ca/jfox/Books/Companion/Filella, I. & Penuelas, J. (1994). The red edge position and shape as indicators of plant chlorophyll content, biomass and hydric status. International journal of remote sensing, 15, 1459–1470.)

848  
849  
850

851 Finegan, B., Peña-Claros, M., de Oliveira, A., Ascarrunz, N., Bret-Harte, M.S., Carreño-  
852 Rocabado, G., Casanoves, F., Díaz, S., Eguiguren Velepucha, P., Fernandez, F., Licona,  
853 J.C., Lorenzo, L., Salgado Negret, B., Vaz, M. & Poorter, L. (2015). Does functional  
854 trait diversity predict above-ground biomass and productivity of tropical forests? Testing  
855 three alternative hypotheses. *The Journal of Ecology*, 103, 191–201.

856 Fuentes-Peailillo, F., Ortega-Farias, S., Rivera, M., Bardeen, M. & Moreno, M. (2018).  
857 Comparison of vegetation indices acquired from RGB and Multispectral sensors placed  
858 on UAV. *2018 IEEE International Conference on Automation/XXIII Congress of the  
859 Chilean Association of Automatic Control (ICA-ACCA)* pp. 1–6. IEEE.

860 Galvão, L.S., Ponzoni, F.J., Liesenberg, V. & Santos, J.R. dos. (2009). Possibilities of  
861 discriminating tropical secondary succession in Amazônia using hyperspectral and  
862 multiangular CHRIS/PROBA data. *International Journal of Applied Earth Observation  
863 and Geoinformation*, 11, 8–14.

864 Gamfeldt, L., Snäll, T., Bagchi, R., Jonsson, M., Gustafsson, L., Kjellander, P., Ruiz-Jaen,  
865 M.C., Fröberg, M., Stendahl, J., Philipson, C.D., Mikusiński, G., Andersson, E.,  
866 Westerlund, B., Andrén, H., Moberg, F., Moen, J. & Bengtsson, J. (2013). Higher levels  
867 of multiple ecosystem services are found in forests with more tree species. *Nature  
868 Communications*, **4**, 1340.

869 Gamon, J.A., Serrano, L. & Surfus, J.S. (1997). The photochemical reflectance index: an  
870 optical indicator of photosynthetic radiation use efficiency across species, functional  
871 types, and nutrient levels. *Oecologia*, **112**, 492–501.

872 Garcia Millan, V. & Sanchez-Azofeifa, A. (2018). Quantifying Changes on Forest Succession  
873 in a Dry Tropical Forest Using Angular-Hyperspectral Remote Sensing. *Remote sensing*,  
874 **10**, 1865.

875 Ghiyamat, A. & Shafri, H.Z.M. (2010). A review on hyperspectral remote sensing for  
876 homogeneous and heterogeneous forest biodiversity assessment. *International journal of  
877 remote sensing*, **31**, 1837–1856.

878 Gitelson, A.A., Kaufman, Y.J., Stark, R. & Rundquist, D. (2002). Novel algorithms for  
879 remote estimation of vegetation fraction. *Remote Sensing of Environment*, **80**, 76–87.

880 Gitelson, A.A., Keydan, G.P. & Merzlyak, M.N. (2006). Three-band model for noninvasive  
881 estimation of chlorophyll, carotenoids, and anthocyanin contents in higher plant leaves.  
882 *Geophysical Research Letters*, **33**.

883 Gitelson, A.A., Zur, Y., Chivkunova, O.B. & Merzlyak, M.N. (2007). Assessing Carotenoid  
884 Content in Plant Leaves with Reflectance Spectroscopy¶. *Photochemistry and*

- 885 *Photobiology*, **75**, 272–281.
- 886 Gonçalves, N.B., Lopes, A.P., Dalagnol, R., Wu, J., Pinho, D.M. & Nelson, B.W. (2020).  
887 Both near-surface and satellite remote sensing confirm drought legacy effect on tropical  
888 forest leaf phenology after 2015/2016 ENSO drought. *Remote Sensing of Environment*,  
889 **237**, 111489.
- 890 Green, A.A., Berman, M., Switzer, P. & Craig, M.D. (1988). A transformation for ordering  
891 multispectral data in terms of image quality with implications for noise removal. *IEEE*  
892 *Transactions on Geoscience and Remote Sensing*, **26**, 65–74.
- 893 Guariguata, M.R. & Evans, K. (2020). A diagnostic for collaborative monitoring in forest  
894 landscape restoration. *Restoration Ecology*, **28**, 742–749.
- 895 Guillemot, J., Kunz, M., Schnabel, F., Fichtner, A., Madsen, C.P., Gebauer, T., Härdtle, W.,  
896 von Oheimb, G. & Potvin, C. (2020). Neighbourhood-mediated shifts in tree biomass  
897 allocation drive overyielding in tropical species mixtures. *The New Phytologist*, **228**,  
898 1256–1268.
- 899 Hernández-Stefanoni, J., Dupuy, J., Johnson, K., Birdsey, R., Tun-Dzul, F., Peduzzi, A.,  
900 Caamal-Sosa, J., Sánchez-Santos, G. & López-Merlín, D. (2014). Improving species  
901 diversity and biomass estimates of tropical dry forests using airborne lidar. *Remote*  
902 *sensing*, **6**, 4741–4763.
- 903 Höhl, M., Ahimbisibwe, V., Stanturf, J.A., Elsasser, P., Kleine, M. & Bolte, A. (2020). Forest  
904 landscape restoration—what generates failure and success? *Forests*, **11**, 938.
- 905 Hu, T., Sun, X., Su, Y., Guan, H., Sun, Q., Kelly, M. & Guo, Q. (2020). Development and  
906 Performance Evaluation of a Very Low-Cost UAV-Lidar System for Forestry  
907 Applications. *Remote sensing*, **13**, 77.
- 908 Huete, A., Didan, K., Miura, T., Rodriguez, E.P., Gao, X. & Ferreira, L.G. (2002). Overview  
909 of the radiometric and biophysical performance of the MODIS vegetation indices.  
910 *Remote Sensing of Environment*, **83**, 195–213.
- 911 Isenburg, M., 2020. LAStools - Efficient LiDAR Processing Software (version 1.8,  
912 Licensed). Obtained from. <http://rapidlasso.com/LAStools>.
- 913 Jia, W., Pang, Y., Tortini, R., Schläpfer, D., Li, Z. & Roujean, J.-L. (2020). A Kernel-Driven  
914 BRDF Approach to Correct Airborne Hyperspectral Imagery over Forested Areas with  
915 Rugged Topography. *Remote sensing*, **12**, 432.
- 916 Jordan, C.F. (1969). Derivation of Leaf-Area Index from Quality of Light on the Forest  
917 Floor. *Ecology*, **50**, 663.
- 918 Keil, P. & Chase, J.M. (2019). Global patterns and drivers of tree diversity integrated across a  
919 continuum of spatial grains. *Nature Ecology & Evolution*, **3**, 390–399.
- 920 Kim, M.S. (1994). THE USE OF NARROW SPECTRAL BANDS FOR IMPROVING  
921 REMOTE SENSING ESTIMATIONS OF FRACTIONALLY ABSORBED  
922 PHOTOSYNTHETICALLY ACTIVE RADIATION. *Digital Repository at the*  
923 *University of Maryland*.

- 924 Kotivuori, E., Kukkonen, M., Mehtätalo, L., Maltamo, M., Korhonen, L. & Packalen, P.  
925 (2020). Forest inventories for small areas using drone imagery without in-situ field  
926 measurements. *Remote Sensing of Environment*, **237**, 111404.
- 927 Krůček, M., Král, K., Cushman, K.C., Missarov, A. & Kellner, J.R. (2020). Supervised  
928 Segmentation of Ultra-High-Density Drone Lidar for Large-Area Mapping of Individual  
929 Trees. *Remote sensing*, **12**, 3260.
- 930 Krutz, D., Müller, R., Knodt, U., Günther, B., Walter, I., Sebastian, I., Säuberlich, T.,  
931 Reulke, R., Carmona, E., Eckardt, A., Venus, H., Fischer, C., Zender, B., Arloth, S.,  
932 Lieder, M., Neidhardt, M., Grote, U., Schrandt, F., Gelmi, S. & Wojtkowiak, A. (2019).  
933 The instrument design of the DLR earth sensing imaging spectrometer (DESIS). *Sensors*  
934 (*Basel, Switzerland*), **19**.
- 935 Laliberté, E., Schweiger, A.K. & Legendre, P. (2020). Partitioning plant spectral diversity  
936 into alpha and beta components. *Ecology Letters*, **23**, 370–380.
- 937 Lasky, J.R., Uriarte, M., Boukili, V.K., Erickson, D.L., John Kress, W. & Chazdon, R.L.  
938 (2014). The relationship between tree biodiversity and biomass dynamics changes with  
939 tropical forest succession. *Ecology Letters*, **17**, 1158–1167.
- 940 Lin, Q., Huang, H., Wang, J., Huang, K., Liu, Y., 2019. Detection of Pine Shoot Beetle (PSB)  
941 Stress on Pine Forests at Individual Tree Level using UAV-Based Hyperspectral  
942 Imagery and Lidar. *Remote Sensing*, **11**, 2540. MacArthur, R.H. & Horn, H.S. (1969).  
943 Foliage Profile by Vertical Measurements. *Ecology*, **50**, 802.
- 944 Marselis, S.M., Abernethy, K., Alonso, A., Armston, J., Baker, T.R., Bastin, J., Bogaert, J.,  
945 Boyd, D.S., Boeckx, P., Burslem, D.F.R.P., Chazdon, R., Clark, D.B., Coomes, D.,  
946 Duncanson, L., Hancock, S., Hill, R., Hopkinson, C., Kearsley, E., Kellner, J.R.,  
947 Kenfack, D. & Dubayah, R. (2020). Evaluating the potential of full-waveform lidar for  
948 mapping pan-tropical tree species richness. *Global Ecology and Biogeography*.
- 949 Meneses, P. R., de Almeida, T., & de Mello Baptista, G. M. (2019). Reflectância dos  
950 materiais terrestres. *Oficina de Textos*.
- 951 Mensah, S., Salako, V.K. & Seifert, T. (2020). Structural complexity and large-sized trees  
952 explain shifting species richness and carbon relationship across vegetation types.  
953 *Functional ecology*.
- 954 Palmer, M.W., Earls, P.G., Hoagland, B.W., White, P.S. & Wohlgemuth, T. (2002).  
955 Quantitative tools for perfecting species lists. *Environmetrics (London, Ont.)*, **13**, 121–  
956 137.
- 957 Papa, D. de A., Almeida, D.R.A. de, Silva, C.A., Figueiredo, E.O., Stark, S.C., Valbuena, R.,  
958 Rodriguez, L.C.E. & d’Oliveira, M.V.N. (2020). Evaluating tropical forest classification  
959 and field sampling stratification from lidar to reduce effort and enable landscape  
960 monitoring. *Forest Ecology and Management*, **457**, 117634.
- 961 Peñuelas, J., Baret, F., & Filella, I. (1995). Semiempirical indexes to assess carotenoids  
962 chlorophyll-a ratio from leaf spectral reflectance. *Photosynthetica*, **31**, 221–230.

- 963 Poorter, L., van der Sande, M.T., Thompson, J., Arets, E.J.M.M., Alarcón, A., Álvarez-  
964 Sánchez, J., Ascarrunz, N., Balvanera, P., Barajas-Guzmán, G., Boit, A., Bongers, F.,  
965 Carvalho, F.A., Casanoves, F., Cornejo-Tenorio, G., Costa, F.R.C., de Castilho, C.V.,  
966 Duivenvoorden, J.F., Dutrieux, L.P., Enquist, B.J., Fernández-Méndez, F. & Peña-  
967 Claros, M. (2015). Diversity enhances carbon storage in tropical forests. *Global Ecology*  
968 *and Biogeography*, **24**, 1314–1328.
- 969 Prata, G.A., Broadbent, E.N., de Almeida, D.R.A., St. Peter, J., Drake, J., Medley, P., Corte,  
970 A.P.D., Vogel, J., Sharma, A., Silva, C.A., Zambrano, A.M.A., Valbuena, R. &  
971 Wilkinson, B. (2020). Single-Pass UAV-Borne GatorEye LiDAR Sampling as a Rapid  
972 Assessment Method for Surveying Forest Structure. *Remote sensing*, **12**, 4111.
- 973 Price, J.C. (1994). How unique are spectral signatures? *Remote Sensing of Environment*, **49**,  
974 181–186.
- 975 R Core Team (2020). R: a language and environment for statistical computing. R Foundation  
976 for Statistical Computing website.
- 977 Richter, R., Reu, B., Wirth, C., Doktor, D. & Vohland, M. (2016). The use of airborne  
978 hyperspectral data for tree species classification in a species-rich Central European forest  
979 area. *International Journal of Applied Earth Observation and Geoinformation*, **52**, 464–  
980 474.
- 981 Rocchini, D., Balkenhol, N., Carter, G.A., Foody, G.M., Gillespie, T.W., He, K.S., Kark, S.,  
982 Levin, N., Lucas, K., Luoto, M., Nagendra, H., Oldeland, J., Ricotta, C., Southworth, J.  
983 & Neteler, M. (2010). Remotely sensed spectral heterogeneity as a proxy of species  
984 diversity: Recent advances and open challenges. *Ecological informatics*, **5**, 318–329.
- 985 Rosa, M.R., Brancalion, P.H.S., Crouzeilles, R., Tambosi, L.R., Piffer, P.R., Lenti, F.E.B.,  
986 Hirota, M., Santiami, E. & Metzger, J.P. (2021). Hidden destruction of older forests  
987 threatens Brazil's Atlantic Forest and challenges restoration programs. *Science*  
988 *Advances*, **7**.
- 989 Rouse, J. W., Haas, R. H., Schell, J. A., & Deering, D. W. (1974). Monitoring vegetation  
990 systems in the Great Plains with ERTS. NASA special publication, 351, 309.
- 991 Roussel, J., & Auty, D. (2019). lidR: Airborne LiDAR data manipulation and visualization  
992 for forestry applications. R package version 2.0.0.
- 993 Sankey, T., Donager, J., McVay, J., Sankey, J.B., 2017. UAV lidar and hyperspectral fusion  
994 for forest monitoring in the southwestern USA. *Remote Sensing of Environment*, **195**,  
995 30–43.
- 996 Silva, C., Hudak, A., Vierling, L., Klauberg, C., Garcia, M., Ferraz, A., Keller, M., Eitel, J.,  
997 & Saatchi, S. (2017). Impacts of airborne lidar pulse density on estimating biomass  
998 stocks and changes in a selectively logged tropical forest. *Remote Sensing*, **9**, 1068.
- 999 Silva Junior, C.H.L., Heinrich, V.H.A., Freire, A.T.G., Broggio, I.S., Rosan, T.M., Doblás, J.,  
1000 Anderson, L.O., Rousseau, G.X., Shimabukuro, Y.E., Silva, C.A., House, J.I. & Aragão,  
1001 L.E.O.C. (2020). Benchmark maps of 33 years of secondary forest age for Brazil.  
1002 *Scientific data*, **7**, 269.

- 1003 Tsanni, A. (2020). African scientists leverage open hardware. *Nature*, **582**, 138.
- 1004 Tsitsi, B. (2016). Remote sensing of aboveground forest biomass: A review. *Tropical*  
1005 *Ecology*, *57*, 125-132.
- 1006 Turner, D.P., Cohen, W.B., Kennedy, R.E., Fassnacht, K.S. & Briggs, J.M. (1999).  
1007 Relationships between Leaf Area Index and Landsat TM Spectral Vegetation Indices  
1008 across Three Temperate Zone Sites. *Remote Sensing of Environment*, **70**, 52–68.
- 1009 Vaglio Laurin, G., Chen, Q., Lindsell, J.A., Coomes, D.A., Frate, F.D., Guerriero, L., Pirotti,  
1010 F. & Valentini, R. (2014). Above ground biomass estimation in an African tropical forest  
1011 with lidar and hyperspectral data. *ISPRS Journal of Photogrammetry and Remote*  
1012 *Sensing*, **89**, 49–58.
- 1013 Vaglio Laurin, G., Puletti, N., Hawthorne, W., Liesenberg, V., Corona, P., Papale, D., Chen,  
1014 Q. & Valentini, R. (2016). Discrimination of tropical forest types, dominant species, and  
1015 mapping of functional guilds by hyperspectral and simulated multispectral Sentinel-2  
1016 data. *Remote Sensing of Environment*, **176**, 163–176.
- 1017 Valbuena, R., Hernando, A., Manzanera, J.A., Görgens, E.B., Almeida, D.R.A., Mauro, F.,  
1018 García-Abril, A. & Coomes, D.A. (2017). Enhancing of accuracy assessment for forest  
1019 above-ground biomass estimates obtained from remote sensing via hypothesis testing  
1020 and overfitting evaluation. *Ecological Modelling*, **366**, 15–26.
- 1021 Valbuena, R., O’Connor, B., Zellweger, F., Simonson, W., Vihervaara, P., Maltamo, M.,  
1022 Silva, C.A., Almeida, D.R.A., Danks, F., Morsdorf, F., Chirici, G., Lucas, R., Coomes,  
1023 D.A. & Coops, N.C. (2020). Standardizing Ecosystem Morphological Traits from 3D  
1024 Information Sources. *Trends in Ecology & Evolution*, **35**, 656–667.
- 1025 van den Berg, A.K. & Perkins, T.D. (2005). Nondestructive estimation of anthocyanin  
1026 content in autumn sugar maple leaves. *HortScience*, **40**, 685–686.
- 1027 Vangi, E., D’Amico, G., Francini, S., Giannetti, F., Lasserre, B., Marchetti, M. & Chirici, G.  
1028 (2021). The new hyperspectral satellite PRISMA: imagery for forest types  
1029 discrimination. *Sensors (Basel, Switzerland)*, **21**.
- 1030 Versluijs, M., Hjältén, J. & Roberge, J.-M. (2019). Ecological restoration modifies the value  
1031 of biodiversity indicators in resident boreal forest birds. *Ecological Indicators*, **98**, 104–  
1032 111.
- 1033 Viani, R.A.G., Barreto, T.E., Farah, F.T., Rodrigues, R.R. & Brancalion, P.H.S. (2018).  
1034 Monitoring young tropical forest restoration sites: how much to measure? *Tropical*  
1035 *Conservation Science*, **11**, 194008291878091.
- 1036 Wanner, W., Li, X. & Strahler, A.H. (1995). On the derivation of kernels for kernel-driven  
1037 models of bidirectional reflectance. *Journal of Geophysical Research*, **100**, 21077.
- 1038 White, J.C., Wulder, M.A., Hermosilla, T. & Coops, N.C. (2019). Satellite time series can  
1039 guide forest restoration. *Nature*, **569**, 630.
- 1040 Williams, L.J., Cavender-Bares, J., Townsend, P.A., Couture, J.J., Wang, Z., Stefanski, A.,  
1041 Messier, C. & Reich, P.B. Remote spectral detection of biodiversity effects on forest

- 1042 biomass. *Nature Ecology & Evolution*, **5**, 46–54.
- 1043 Williams, L.J., Paquette, A., Cavender-Bares, J., Messier, C. & Reich, P.B. (2017). Spatial  
1044 complementarity in tree crowns explains overyielding in species mixtures. *Nature*  
1045 *Ecology & Evolution*, **1**, 63.
- 1046 Wortley, L., Hero, J.-M. & Howes, M. (2013). Evaluating Ecological Restoration Success: A  
1047 Review of the Literature. *Restoration Ecology*, **21**, 537–543.
- 1048 Wulder, M.A., White, J.C., Nelson, R.F., Næsset, E., Ørka, H.O., Coops, N.C., Hilker, T.,  
1049 Bater, C.W. & Gobakken, T. (2012). Lidar sampling for large-area forest  
1050 characterization: A review. *Remote Sensing of Environment*, **121**, 196–209.
- 1051 Yan, J., Zhou, W., Han, L. & Qian, Y. (2018). Mapping vegetation functional types in urban  
1052 areas with WorldView-2 imagery: Integrating object-based classification with  
1053 phenology. *Urban Forestry & Urban Greening*, **31**, 230–240.
- 1054 Zellweger, F., Baltensweiler, A., Schleppi, P., Huber, M., Kuchler, M., Ginzler, C. & Jonas,  
1055 T. (2019). Estimating below-canopy light regimes using airborne laser scanning: An  
1056 application to plant community analysis. *Ecology and Evolution*, **9**, 9149–9159.
- 1057 Zhao, Y., Zeng, Y., Zheng, Z., Dong, W., Zhao, D., Wu, B. & Zhao, Q. (2018). Forest  
1058 species diversity mapping using airborne LiDAR and hyperspectral data in a subtropical  
1059 forest in China. *Remote Sensing of Environment*, **213**, 104–114.
- 1060